[American Journal of Science, Vol. 314, January, 2014, P. 80–109, DOI 10.2475/01.2014.03]

POST-ACCRETIONARY PERMIAN GRANITOIDS IN THE CHINESE ALTAI OROGEN: GEOCHRONOLOGY, PETROGENESIS AND TECTONIC IMPLICATIONS

YING TONG*,†, TAO WANG*, BOR-MING JAHN**, MIN SUN***, DA-WEI HONG*, and JIAN-FENG GAO***

ABSTRACT. The Altai orogen is an important constituent of the Central Asian Orogenic Belt (CAOB). The main orogenic processes occurred mainly in the early to middle Paleozoic and involved a series of northward subduction and terrane accretion. However, termination of the accretionary and post-accretionary processes remains poorly defined. The Chinese Altai is located in the southern part of this orogeny, which is widely intruded by Permian granitic plutons. These plutons are approximately circular in shape, free of deformation and generally cutting pre-Permian structures, suggesting a post-tectonic formation. We report the results of geochronological and geochemical data from five specific granitic plutons (Buerjin, Xibodu, Daqiaonan, Aweitan, and Adenbluk), which all yielded magmatic zircon U-Pb ages of about 270 Ma. These plutons are composed of high-K calc-alkaline rocks, including K-feldspar megaphyric granite, biotite granite and monzogranite that have metaluminous to weakly LREE-enriched, coupled with negative Eu anomalies. Significant negative anomalies of Ba, Sr, P, and Ti are also observed in the primitive-mantle normalized diagram. They have positive whole-rock $\varepsilon_{Nd}(t)$ (+1.3 to +7.2) and zircon $\varepsilon_{Hf}(t)$ values (+5.6 to +12.9), yielding Sm-Nd model ages of ≤0.9 Ga. Therefore, these granitoids are proposed to have been generated by differentiation of mantle-derived magmas with variable crustal contamination. In view of the field occurrence, structural analysis, regional tectonics and geochemical characteristics, these Permian plutons are concluded to be post-accretionary or post-collisional. Asthenospheric upwelling after the collision and amalgamation of the Altai and Junggar blocks could have caused the mantle-derived magmas that evolved to form the granitoids. We note that Permian intrusions are not only widespread but also voluminous in the CAOB. They mostly are post-collisional products, and some of them might have been related to the large igneous province activity in the Tarim Block.

Key words: Altai, zircon U-Pb age, granitoids, Permian, post-collisional, CAOB (Central Asian Orogenic Belt)

INTRODUCTION

The Central Asian Orogenic Belt (CAOB) (Jahn and others, 2000a), otherwise known as the Altaids, or the Central Asian Mobile Belt, or the Central Asian Fold Belt (Şengör and others, 1993; Yakubchuk, 2004; Kovalenko and others, 2004), is located between the Siberian Craton to the north, the East European Craton to the west and the Tarim and North China Cratons to the south (inset of fig. 1). The CAOB is one of the largest and most typical accretionary collages on the Earth evolved from late Proterozoic to Mesozoic (Şengör and Natal'in, 1996; Jahn and others, 2000a, 2000b; Windley and others, 2002, 2007; Jahn, 2004; Kröner and others, 2007; Xiao and others, 2009a). Recent investigations have revealed that the CAOB is composed of multiple ancient microcontinental fragments, island arcs, seamounts, ophiolites, and other lithotectonic units (Windley and others, 2002; Khain and others, 2003; Xiao and others, 2003, 2004, 2009b; Wilhem and others, 2012; Kröner and others, 2013). During

* Institute of Geology, Chinese Academy of Geological Sciences, Baiwanzhuang Road 26, Beijing, 100037, P. R. China
** Department of Geosciences, National Taiwan University, Taipei 106, Taiwan
*** Department of Earth Sciences, The University of Hong Kong, Pokfulam Road, Hong Kong, China
† Corresponding author: yingtong@cags.ac.cn; Tel: +86-10-68999732, Fax: +86-10-68997803

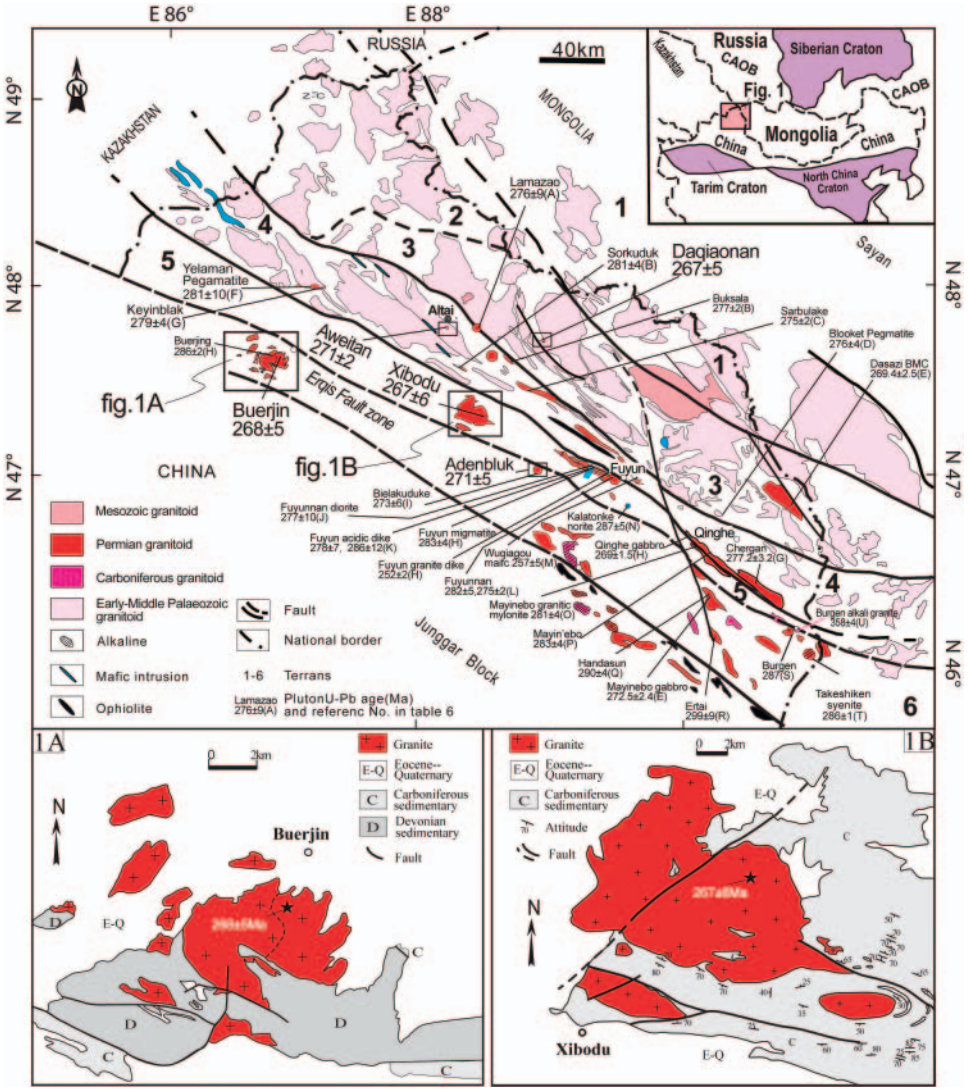

Fig. 1. Simplified geological map of the Chinese Altai and more detail maps of the Buerjin (fig. 1A) and Xibodu (fig. 1B) granitic plutons. Tectonic subdivision modified from Windley and others (2002). Permian intrusions are marked by their zircon ages. Data sources: *A*, Wang and others (2005); *B*, Gao and others (2010); *C*, Sun and others (2009a); *D*, Ren and others (2011); *E*, Zhang and others (2010b); *F*, Sun and others (2009b); *G*, Li and others (2012); *H*, Zhang and others (2012); *I*, Han and others (2006); *J*, Gong and others (2007); *K*, Briggs and others (2007); *L*, Tong and others (2006b); *M*, Chen and Han (2006); *N*, Han and others (2004); *O*, Zhou and others (2007a); *P*, Zhou and others (2007b); *Q*, Zhou and others (2009); *R*, Li and others (2004); *S*, Liu and others (1996); *T*, Tong and others (2006b); *U*, Tong and others (2012). Detailed data can be seen in table 6.

the CAOB evolution, small orogens formed through subduction, mostly northward, of small ocean basins (Xiao and others, 2010). It is critical to define the tectonic nature and evolution of individual small orogens in order to better understand the tectonic evolution of the CAOB.

The Altai (or Altay) orogen is located in the center of the CAOB. To the south it is separated from the Junggar block by the Erqis Fault and to the north it is bordered by

the Sayan and associated orogenic belts (fig. 1). The Altai orogen extends from Russia, Kazakhstan, via North Xinjiang (the Chinese Altai) to Mongolia. The Chinese Altai, lying in the south margin of Altai orogen, defines an important segment of the Altai orogenic belt. Generally, the Altai orogen was considered to be an early-middle Paleozoic subduction-accretionary regime (Wang and others, 2006; Sun and others, 2008; Long and others, 2010; Wang and others, 2011) with a *ca.* 400 Ma peak in magmatism (Tong and others, 2007; Cai and others, 2011a). However, a number of issues regarding the tectonic processes at the final stage of orogenesis remain unresolved; such as, (1) did the subduction/accretionary process last throughout the Paleozoic time? And (2) when was the accretionary process completely terminated?

Granitic plutons were widely emplaced in the Chinese Altai from early Paleozoic to Mesozoic (Wang and others, 2010). The early-middle Paleozoic granitoids have been studied in great detail (Wang and others, 2006; Tong and others, 2007; Yuan and others, 2007; Sun and others, 2008; Cai and others, 2011b; and references therein), but investigation on the late Paleozoic plutons was very limited. This paper presents our new geochronological and geochemical dataset of five Permian granitic plutons from the Chinese Altai. The results will then be used to discuss the granite petrogenesis and regional tectonic implications.

GEOLOGICAL SETTING

The Chinese Altai consists of variably deformed meta-sedimentary, volcanic rocks and granitic intrusions. Depending on the authors, this region consists of several "terranes" (Windley and others, 2002) or "tectonic units" (He and others, 1990; Li and others, 2003; Xiao and others, 2004). However, Wang and others (2009a) proposed to divide the region into three NW-SE-trending units.

The northern unit (= terrane 1 of Windley and others, 2002) consists of middle-late Devonian andesites, dacites and late Devonian to early Carboniferous (?) meta-sediments (shale, siltstone, graywacke, sandstone, limestone).

The central unit (= terranes 2 and 3) consists of Neoproterozoic to middle-late Ordovician low-grade meta-sedimentary and volcanic rocks of the Habahe Group in the northwest (Shan and others, 2005; Long and others, 2007, 2008, 2010), and Ordovician to Silurian amphibolite and greenschist-facies meta-sediments and meta-volcanics in the southwest (Jiang and others, 2010).

The southern unit consists of terranes 4, 5 and 6. Traditionally, this unit contains two formations: the Kangbutiebao and Altai Formations. The Kangbutiebao Formation consists of arc-type volcanic and pyroclastic rocks, and minor basic volcanic rocks and spilites. This formation was considered to be deposited during late Silurian to early Devonian (Zhang and others, 2000; Chai and others, 2008, 2009), whereas the Altai Formation is composed predominantly of low-grade meta-turbidite sequences, minor basalts, siliceous volcanics and limestones. The limestones contain middle Devonian fossils. Based on the field occurrence and geochemical studies of clastic and volcanic rocks, the two formations were probably formed in a fore-arc basin (Windley and others, 2002; Long and others, 2007, 2008). In addition, magmatic rocks of adakitic composition, mafic complexes, high-Mg andesites and boninites are also developed in this area (Xu and others, 2003; Niu and others, 2006; Wong and others, 2010; Cai and others, 2012). All these features indicated an active continental margin (Şengör and others, 1993; Yuan and others, 2007).

The Erqis (other spellings: Irtysh, Ertix, Erqishi, Irtish, Irtishi) Fault is one of the largest strike-slip faults in Asia and an important structure element in the tectonic framework of CAOB. It extends for more than 1000 km into Mongolia and Kazakhstan. The fault zone can reach a width of up to 50 km and it separates the Altai orogen from the Junggar Block in the south (Şengör and others, 1993; Buslov and others, 2004; Buslov, 2011). The NW trending fault underwent a right-lateral movement during late

Carboniferous-Permian times (Laurent-Charvet and others, 2003; Tong and others, 2006a; Zhou and others, 2007a; Briggs and others, 2007, 2009).

Based on the available zircon U-Pb ages, the granitic and mafic intrusions in the Chinese Altai can be divided into three intrusive phases: early-middle Paleozoic, late Paleozoic, and Mesozoic (Wang and others, 2010; Cai and others, 2011a; and references therein). Amongst the granitoids, the early-middle Paleozoic ones make up more than 80 percent of the intrusions and 70 percent of the exposed rocks (fig. 1).

FIELD OCCURRENCE AND PETROGRAPHY

In recent years we have studied 35 intrusions at the Chinese Altai. Seventeen of them have been published for their whole rock geochemistry and U-Pb age (Wang and others, 2005, 2006, 2013; Tong and others, 2005, 2006a, 2006b, 2007, 2012). This paper is going to report five granitoids at Buerjin, Xibodu, Daqiaonan, Aweitan and Adenbluk of the south unit (fig. 1).

Buerjin pluton.—This granite pluton, located in the western part of the south unit, is the largest pluton in the Jimunai-Buerjin area (fig. 1A). Intrusive contacts are preserved in the south between this pluton and the late Devonian Altai Formation, whereas the northern part of the pluton is covered by the Tertiary and Quaternary sediments. Small pale red K-feldspar granite veins were intruded into the Buerjin pluton. The pluton exhibits a medium-grained porphyric biotite monzogranite facies. Most phenocrysts are K-feldspar, and some show well-developed zonal structure. Dark dioritic enclaves and wall rock xenoliths are observed in the pluton. Samples were collected from fresh outcrops (quarry) of the southern part of the pluton. Their major minerals are plagioclase (25-30%), K-feldspar (30-35%), quartz (25-30%) and biotite (5-10%). Accessory minerals include zircon, magnetite and sphene.

Xibodu pluton.—This pluton is located in the southern Altai orogen, near the Xibodu Ferry of the Erqis River. It is ellipsoidal and intrusive into folded Carboniferous (?) garnet biotite plagioclase gneiss (fig. 1B). The pluton sharply cut the foliations of the wall rocks essentially without contact metamorphic effects (fig. 2A). No deformation has been obtained within the pluton. The rock types of the pluton are mainly red coarse monzogranite. A few microgranular granodioritic enclaves and wall rock xenoliths are occasionally observed in the pluton. The essential minerals of the main body granite (monzogranite) include plagioclase (30-35%), K-feldspar (25-30%), quartz (20-25%) and biotite (10-15%). Accessories are garnet, titanite, magnetite and zircon.

Daqiaonan pluton.—This pluton occurs in the south of the Aletai Black Bridge (~40 km east to the Aletai city). It was intruded into the highly deformed Devonian Wuliqi gneissic granite (375 Ma, Wang and others, 2006) with a strong foliation and a lineation parallel to the regional foliation. The Daqiaonan pluton itself is undeformed and shows post-tectonic characteristics. It consists mainly of medium- to fine-grained biotite granites. Rock forming minerals are plagioclase (40-45%), alkaline feldspar (15-20%), quartz (30-35%) and biotite (3-5%); accessory minerals are magnetite and zircon.

Aweitan pluton.—The body of this pluton is situated to the southeast of the Aletai city. This pluton intrudes the strongly deformed Devonian Aweitan granitic gneiss (400 Ma, Wang and others, 2006) and cuts the gneissic foliation of this body that is parallel to the regional NW-trending foliation. The Aweitan pluton is K-feldspar megaphyric granite and composed of alkali feldspar (50-55%), plagioclase (10-15%), quartz (20-25%) and biotite (−5%), with minor zircon and apatite.

Adenbluk pluton.—This pluton is located south of the Erqis River (fig. 1). It has been "flat-topped" by weathering and erosion. Plenty of small granite outcrops are scattered in the Gobi desert and do not unveil the overall shape, but the circular form is clearly visible on the satellite image (fig. 2B). The Adenbluk pluton is undeformed

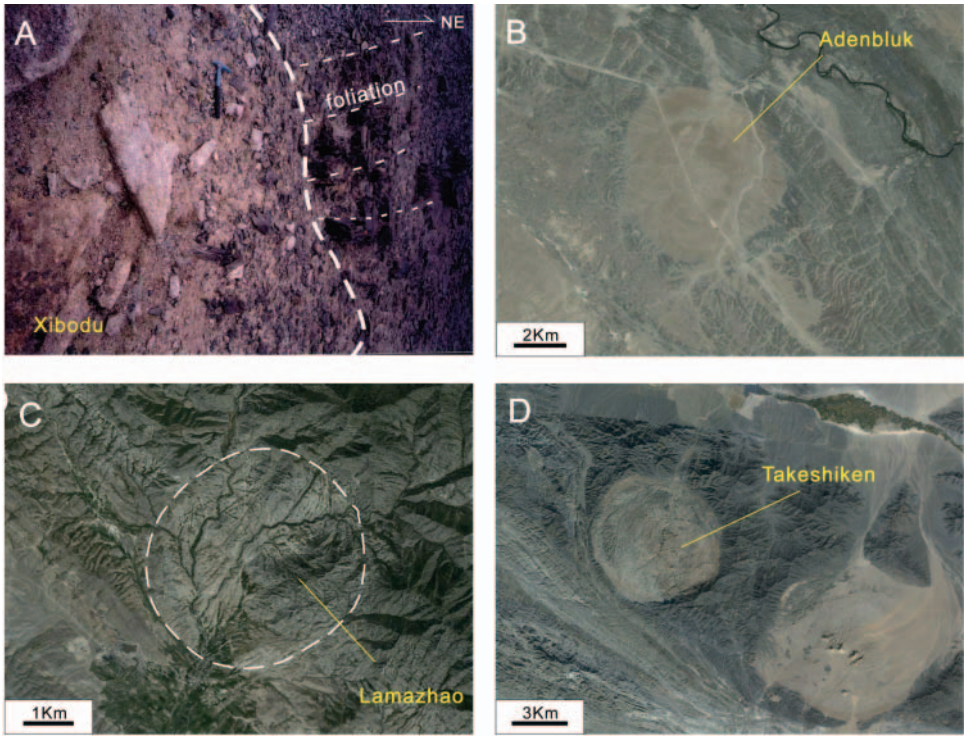

Fig. 2. Field and satellite photographs of the Permian plutons. (A) The Xibodu pluton cut the foliations of the deformed strata; (B) circular shape of the Adenbluk pluton; (C) the rounded Lamazhao pluton cutting the fault and old tectonic lineament; (D) two round plutons intruded the strata in the East of Erqis zone; the left is the Takeshiken syenite, which shows the typical post-kinematic characters. Satellite photos are obtained from http://maps.google.com/.

and consists of coarse-grained porphyritic hornblende monzogranites. The pluton contains numerous enclaves with feldspar phenocrysts. Moreover, numerous radial dikes were intruded into this pluton, and most of which are aplites to quartz-porphyries.

ANALYTICAL METHODS

U-Pb zircon geochronology.—Cathodoluminescence (CL) imaging of polished zircons embedded in epoxy was conducted on a JEOL scanning electron microscope. Three different methods for U-Pb isotope analyses were employed: (1) LA-ICP-MS *in-situ* zircon analysis was carried out on an Agilent 7500A ICP-MS, equipped with a GeoLas 200M laser ablation system (MicroLas, Göttingen, Germany), at the Key Laboratory of Continental Dynamics, Northwest University, Xi'an. The spot size was 30 μm. Zircon 91500 and glass standard NIST SRM 610 were used as external standards for the age and concentration calculation, respectively, and ^{29}Si (32.8% SiO_2) was chosen as the internal standard. Isotope ratios and elemental concentrations were calculated and plotted using the GLITTER 4.0 software (Macquarie University). For common Pb correction, the software of Andersen (2002) was employed, and the age calculations were performed with Isoplot 3.0 (Ludwig, 2003); (2) SRHIMP, zircon U-Pb dating was performed at the Beijing SHRIMP center of the Chinese Academy of Geological Sciences, using the standard operating condition (Williams, 1998). U-Th-Pb isotopic ratios were determined relative to the TEMORA standard zircon (Black and

TABLE 1

Zircon U-Pb isotopic analytical data of Buerjin, Xibodu and Daqiaonan plutons

No.	$\%^{206}Pb_c$	U ppm	Th ppm	$^{206}Pb^*$ ppm	$\frac{^{232}Th}{^{238}U}$	$\frac{^{207}Pb^*}{^{206}Pb^*}$	1σ	$\frac{^{207}Pb^*}{^{235}U}$	1σ	$\frac{^{206}Pb^*}{^{238}U}$	1σ	$^{206}Pb/^{238}U$ (Ma)	±	$^{208}Pb/^{232}Th$ (Ma)	±
Buerjin monzogranite(3198, LA-ICP-MS)															
1	0.00	910.17	577.55	81.63	0.29	0.18003	0.00180	1.01613	0.01738	0.04093	0.00070	259	4	1414	18
2	0.00	225.01	103.26	23.92	0.20	0.05227	0.00053	0.34106	0.00604	0.04731	0.00082	298	6	297	4
3	1.11	1045.19	809.57	56.60	0.58	0.06987	0.00141	0.38928	0.01404	0.04041	0.00074	255	4	246	4
4	1.80	775.19	458.65	68.48	0.32	0.05220	0.00105	0.34211	0.01246	0.04753	0.00082	299	6	299	6
5	0.00	1486.56	1053.39	100.66	0.49	0.05613	0.00056	0.36249	0.00618	0.04683	0.00080	295	4	285	4
6	0.00	616.14	422.87	45.28	0.44	0.05274	0.00053	0.34109	0.00582	0.04690	0.00080	295	4	281	4
7	0.40	577.66	434.22	33.81	0.56	0.05302	0.00114	0.31797	0.01250	0.04350	0.00078	274	4	274	4
8	0.25	719.42	486.73	50.82	0.41	0.05341	0.00099	0.31753	0.01032	0.04311	0.00076	272	4	271	4
9	0.15	719.76	406.33	67.44	0.26	0.05271	0.00083	0.30949	0.00812	0.04259	0.00074	269	4	268	4
10	0.69	789.04	493.87	63.82	0.33	0.05388	0.00096	0.31563	0.00972	0.04248	0.00074	268	4	267	4
11	0.71	390.56	276.76	25.89	0.45	0.05338	0.00107	0.30680	0.01100	0.04168	0.00074	263	4	262	4
12	0.00	760.37	535.66	55.73	0.44	0.05881	0.00059	0.37319	0.00636	0.04602	0.00078	290	4	337	4
13	0.87	701.13	519.79	42.92	0.53	0.05397	0.00115	0.32207	0.01254	0.04328	0.00076	273	4	272	4
14	3.09	838.12	576.19	59.78	0.41	0.05383	0.00134	0.30533	0.01414	0.04114	0.00074	260	4	258	4
15	0.43	736.54	490.27	51.02	0.41	0.05577	0.00101	0.32604	0.01040	0.04240	0.00074	268	4	265	4
16	1.20	864.00	561.29	69.11	0.34	0.05454	0.00102	0.31309	0.01038	0.04163	0.00074	263	4	261	4
17	1.01	256.65	168.48	20.04	0.38	0.33929	0.00432	2.08291	0.03802	0.04453	0.00080	281	4	232	4
18	0.22	1155.30	757.31	91.55	0.39	0.05398	0.00096	0.34886	0.01088	0.04688	0.00082	295	6	294	4
19	0.88	963.25	674.02	62.75	0.46	0.05390	0.00110	0.31752	0.01164	0.04272	0.00076	270	4	268	4
20	0.03	1024.18	647.05	87.80	0.34	0.05430	0.00054	0.34951	0.00596	0.04668	0.00080	294	4	294	4
Xibodu monzogranite(3055, LA-ICP-MS)															
1	0.00	609.03	476.48	32.90	0.70	0.05748	0.00116	0.38113	0.00658	0.04809	0.00082	303	6	328	4
2	0.00	374.77	299.40	18.04	0.77	0.05423	0.00110	0.34864	0.00600	0.04662	0.00080	294	4	305	4
3	0.59	550.44	376.79	27.32	0.65	0.05259	0.00246	0.33873	0.01464	0.04671	0.00080	294	6	294	4
4	0.39	146.42	120.11	6.46	0.87	0.05358	0.00292	0.34608	0.01770	0.04684	0.00080	295	6	294	4
5	2.71	321.73	233.47	23.47	0.43	0.05419	0.00260	0.31078	0.01386	0.04159	0.00074	263	4	261	4
6	0.00	658.05	447.98	50.48	0.42	0.05716	0.00114	0.37288	0.00642	0.04730	0.00082	298	6	330	4
7	0.00	926.38	723.54	48.56	0.67	0.05119	0.00388	0.29992	0.02198	0.04249	0.00078	268	6	269	4
8	5.45	730.27	550.04	45.35	0.55	0.05311	0.00394	0.31464	0.02252	0.04297	0.00080	271	6	270	6
9	5.84	363.64	281.77	19.54	0.66	0.05818	0.00116	0.36955	0.00642	0.04605	0.00080	290	4	314	4
10	0.00	415.53	314.06	25.51	0.57	0.05646	0.00112	0.35835	0.00624	0.04602	0.00080	290	4	284	4
11	0.00	404.60	316.82	20.93	0.68	0.05441	0.00268	0.33716	0.01528	0.04495	0.00080	283	6	282	4
12	0.67	502.31	251.10	17.30	0.69	0.05233	0.00104	0.34269	0.00596	0.04749	0.00084	299	6	286	4
13	0.00	607.66	530.40	18.89	1.35	0.05240	0.00104	0.34763	0.00604	0.04810	0.00084	303	6	274	4
14	0.00	658.77	476.85	46.74	0.49	0.05531	0.00252	0.35676	0.01488	0.04678	0.00084	295	6	293	6
15	1.81	343.39	269.24	18.40	0.69	0.05250	0.00104	0.34309	0.00598	0.04739	0.00084	298	6	283	4
16	0.00	562.99	429.61	36.29	0.58	0.05299	0.00378	0.34158	0.02344	0.04675	0.00088	295	6	294	6
17	5.29	547.10	430.81	29.50	0.67	0.06753	0.00802	0.36913	0.04310	0.03964	0.00082	251	6	243	8
18	13.40	514.22	415.89	23.90	0.86	0.05852	0.00114	0.40009	0.00700	0.04958	0.00088	312	6	303	4
19	0.00	362.68	292.38	17.60	0.81	0.05321	0.00104	0.35705	0.00626	0.04868	0.00088	306	6	285	4
Daqiaonan biotite granite(152,SHRIMP)															
1	1.81	242.00	110.00	0.47	9.07	0.0383	0.0046	0.227	0.030	0.0429	0.0013	270.6	8	216	23
2	4.55	125.00	79.00	0.66	4.72	0.0189	0.0085	0.109	0.049	0.0419	0.0014	264.6	8.6	192	29
3	1.44	173.00	141.00	0.84	6.41	0.0454	0.0050	0.266	0.029	0.0425	0.0015	268.5	9.3	280	17
4	1.85	113.00	65.00	0.60	4.14	0.0484	0.0053	0.279	0.033	0.0418	0.0018	264	11	246	22
5	0.04	603.00	62.00	0.11	23.40	0.0529	0.0016	0.328	0.013	0.0451	0.0013	284.2	8.1	358	25
6	3.36	193.00	136.00	0.72	7.03	0.031	0.0105	0.176	0.060	0.0409	0.0013	258.6	8.5	208	31
7	3.78	144.00	112.00	0.81	5.77	0.024	0.0103	0.147	0.063	0.0449	0.0020	283	12	207	31
8	2.45	224.00	143.00	0.66	8.30	0.0326	0.0082	0.189	0.047	0.0421	0.0013	265.5	8.2	220	27
9	1.45	174.00	158.00	0.94	5.68	0.0397	0.0040	0.205	0.023	0.0375	0.0012	237.1	7.6	231	12
10	6.75	75.00	67.00	0.92	2.77					0.0401	0.0015	253.5	9.6	157	38
11	0.40	966.00	21.00	0.02	35.30	0.0491	0.0015	0.287	0.012	0.0423	0.0012	267.3	7.5		
12	1.78	111.00	65.00	0.60	3.99	0.0425	0.0051	0.242	0.029	0.0413	0.0014	260.8	8.5	264	20
13	3.04	125.00	81.00	0.67	4.28	0.0285	0.0094	0.152	0.052	0.0386	0.0014	244.1	8.9	176	29

Errors are 1σ; Pb_c and Pb* indicate the common and radiogenic portions, respectively; Common Pb corrected using measured ^{204}Pb.

others, 2003), and U, Th concentrations were measured relative to SL13. Pb isotope ratios were corrected for common Pb using an average crustal composition (Stacey and Kramers, 1975) appropriate for the age of the mineral. U-Pb isotope data were calculated and plotted using the SQUID (1.02) and Isoplot 3.0 (Ludwig, 2003) software. Individual analyses (table 1) are presented as 1σ error boxes on the concordia diagrams and age uncertainties are quoted at the 95 percent confidence

level (2σ); (3) Isotope dilution-thermal ionization mass spectrometry (ID-TIMS) analyses was performed on a Thermo Finnigan Triton TIMS at Tianjin Institute of Geology and Mineral Resources, following the procedures described by Lu and others (2003). Lead and uranium were separated by anion exchange chromatography and the purified Pb and U were loaded with H_3PO_4 and silica gel on degassed Re-single filaments. Pb isotopic ratios were measured at 1250 to 1350 °C, while the U isotopic ratios were analyzed at 1350 to 1450 °C. Repeated analyses of total procedure blanks during this study were lower than 0.05 ng for Pb and 0.002 ng for U, respectively. Instrumental mass bias was corrected using the standard reference NBS 981. U-Pb analytical data were evaluated using the Pb data program and calculated using Isoplot 3.0 (Ludwig, 2003), and age uncertainties are given at the 95 percent (2σ) confidence level.

Major and trace elements analyses.—Major and trace elements were analyzed at the Key Laboratory of Continental Dynamics of the Northwest University, Xi'an. Major elements were determined by X-ray fluorescence (RIX2100X sequential spectrometer). Fe_2O_3 was analyzed by wet chemical methods. Accuracies of the XRF analyses are better than 5 percent. Trace elements and REE were determined using ICP-MS (Elan 6100 DRC). The analytical accuracies are better than 5 percent for Co, Ni, Zn, Ga, Rb, Y, Zr, Nb, Hf, Ta and LREE, and 5 to 15 percent for other elements.

Sr and Nd isotopic compositions.—Sr-Nd isotopes were analyzed at the Isotope Laboratory of the Institute of Geology and Geophysics, Chinese Academy of Sciences, Beijing. The analytical procedures were described by Qiao (1988). Rb, Sr, Sm and Nd concentrations were obtained by isotope dilution using a mixed ^{87}Rb-^{84}Sr-^{149}Sm-^{150}Nd spike solution. Isotopic ratio measurements were made on a Thermo Finnigan MAT262 multi-collector TIMS. $^{87}Sr/^{86}Sr$ and $^{143}Nd/^{144}Nd$ ratios were normalized to $^{86}Sr/^{88}Sr = 0.1194$ and $^{146}Nd/^{144}Nd = 0.7219$, respectively. The mean of the measured $^{143}Nd/^{144}Nd$ of the La Jolla Nd standard was 0.511863 ± 0.000007 (2σ, n = 6). The definition and calculation of εNd, $f_{Sm/Nd}$, model age T_{DM}, as well as blank values, analytical precision and accuracy of the Sr and Nd isotope data, are listed in the footnote of table 4.

In-situ zircon Hf isotopic analyses.—Zircon Hf isotopic analyses were conducted using a Neptune MC-ICP-MS equipped with a New Wave UP213 laser-ablation microprobe at the Institute of Mineral Resources, Chinese Academy of Geological Sciences, Beijing. The analytical procedures were by Hou and others (2007) and Wu and others (2006). A spot with a beam diameter of 40 or 55 μm was selected depending on the size of the ablated domains. In order to correct the isobaric interferences of ^{176}Lu and ^{176}Yb on ^{176}Hf, $^{176}Lu/^{175}Lu = 0.02658$ and $^{176}Yb/^{173}Yb = 0.796218$ ratios were determined (Chu and others, 2002). For instrumental mass bias correction Yb isotope ratios were normalized to $^{172}Yb/^{173}Yb$ of 1.35274 (Chu and others, 2002) and Hf isotope ratios to $^{179}Hf/^{177}Hf$ of 0.7325 using an exponential law. The mass bias behavior of Lu was assumed to follow that of Yb, mass bias correction protocols are described in Wu and others (2006) and Hou and others (2007). Reference standard zircon GJ1 gave a weighted mean $^{176}Hf/^{177}Hf$ ratio of 0.282000 ± 0.000019 (2σ, n = 11), consistent with previous reported $^{176}Hf/^{177}Hf$ ratio of 0.282013 ± 19 (2σ) (Elhlou and others, 2006).

RESULTS

U-Pb Zircon Ages

The Buerjin pluton.—Zircon grains extracted from sample 3198 are colorless and transparent. Most of them tend to occur as euhedral crystals, usually 150 to 300 μm along long axis. Concentric oscillatory zoning typical of magmatic origin is developed in all crystals. Few grains have premagmatic domains with distinct cores (for example,

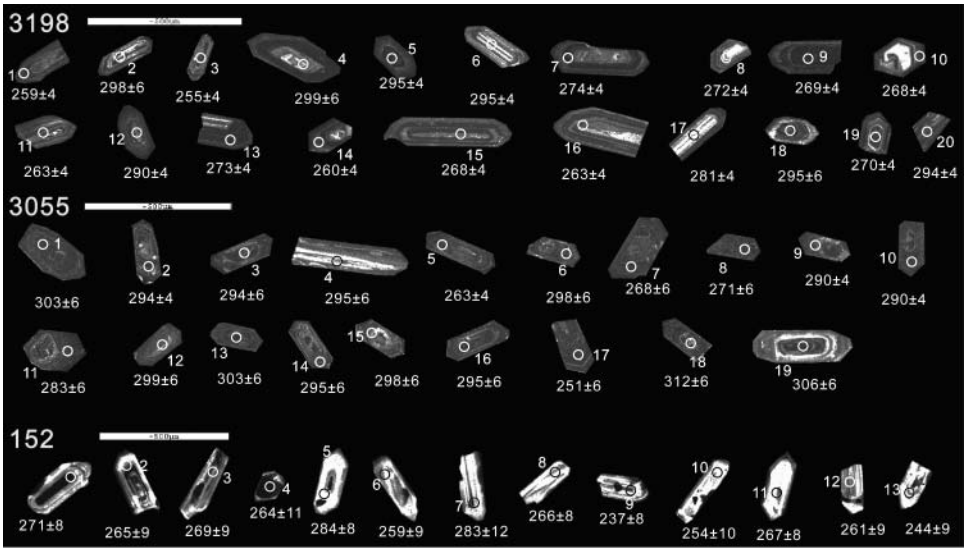

Fig. 3. CL images of zircons from the Buerjin (3198), Xibodu (3055) and Daqiaonan (152) granites.

spot 12, fig. 3). Twenty zircon grains were analyzed by LA-ICPMS. Except for three spots (1, 3, 17) with a high common lead contribution, the remaining seventeen analyses yield two clear age groups: (1) seven spots on zircon core with $^{206}Pb/^{238}U$ ages from 290 Ma to 299 Ma (weighted mean $^{206}Pb/^{238}U$ age = 296 ± 4 Ma), which is similar to that of the Sawure granite which is near the Buerjin pluton; (2) there are ten spots on zircon core and rim with $^{206}Pb/^{238}U$ ages from 260 Ma to 274 Ma (weighted mean $^{206}Pb/^{238}U$ age = 268 ± 5 Ma) (figs. 3 and 4A and table 1). The younger age of 268 ± 5 Ma is considered to be the emplacement age of the host granite, and the zircons dated at 296 ± 4 Ma are either xenocrysts or antecrysts.

The Xibodu pluton.—Most of the zircons from sample 3055 are fine crystals with typical magmatic features but a few have clear inherited core characteristics (fig. 3). Nineteen zircon grains were analyzed by LA-ICPMS. Except for spots 6 and 17 that have a high common Pb component and spot 11 that has an unusually high ^{206}Pb concentration, the data of 16 other spots appear to fall into two age groups. (1) One group has ages between 306 to 290 Ma with a weighted mean $^{206}Pb/^{238}U$ age of 296 ± 3 Ma obtained on 13 spots on zircon cores and rims and (2) three spots on zircon rims with a weighted mean $^{206}Pb/^{238}U$ age of 267 ± 6 Ma (fig. 4B and table 1). The age data are similar to that of sample 3198 of the Buerjin pluton. The analyzed spots with old ages are located on both the rims and the cores and some of these zircons have clear inherited cores. Three points in 19 grains yielded younger ages and all of them were from the rims of grains. It is reasonable to conclude that the older ages observed in inherited cores and rims are all inherited ages whereas the younger weighted mean $^{206}Pb/^{238}U$ age observed only from rims represents the Xibodu pluton's emplacement age.

The Daqiaonan pluton.—The CL images of the zircons from sample 152 are whiter for the low U contains, but most of them have the typical magmatic features that lack inherited cores (fig. 3). Thirteen U-Pb SHRIMP analyses were obtained on zircons. Among them, twelve analyses define a homogeneous age group, yielding a weighted mean $^{206}Pb/^{238}U$ age of 265 ± 5 Ma (MSWD = 1.5) or a more concentrated age of 267 ± 5 Ma (MSWD = 1.0) by excluding one apparent young age (spot 9) (table 1 and

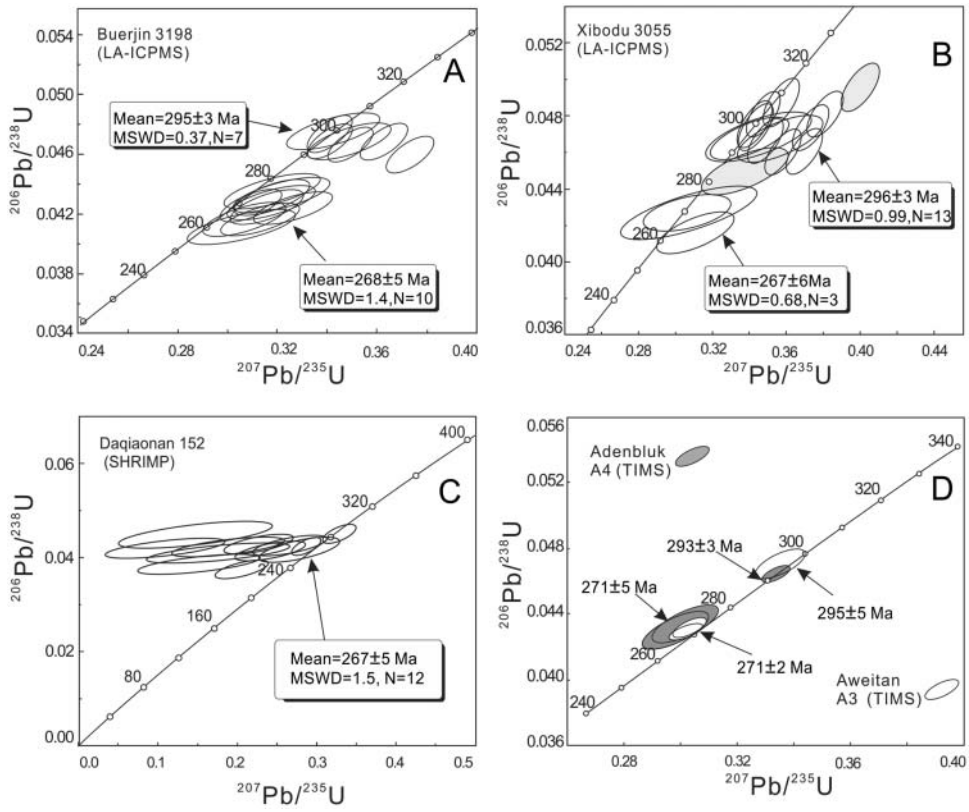

Fig. 4. Zircon U-Pb Concordia diagrams for the Permian granitoids of the Chinese Altai.

fig. 4C). The age of 267 ± 5 Ma is interpreted as the crystallization age of these zircons, and thus, as the formation age of the Daqiaonan pluton.

The Aweitan pluton.—Based on differences in color, shape and transparency, three zircon fractions were prepared for ID-TIMS analyses from sample A3: the first fraction (30 ug) comprises short prismatic, light yellow, translucent euhedral crystals. The zircons in the second and third fractions are also translucent euhedral but bigger than those of the first group. The second fraction (30 ug) comprises long prismatic grains, while the third fraction (35 ug) comprises short prismatic grains. The U-Pb isotope data are listed in table 2, U and Pb concentrations range from 366 to 279 μg/g and 23 to 12 μg/g, respectively. The first fraction yielded a $^{206}Pb/^{238}U$ apparent age of 295 ± 5 Ma, the other two fractions, main part of the zircon grains, display similar $^{206}Pb/^{238}U$ apparent ages with a weighted mean age of 271 ± 2 Ma (hollow error ellipses in fig. 4D), which is more representative and younger and interpreted as the crystallization age of the Aweitan pluton.

The Adenbluk pluton.—Three zircon fractions of sample A4 were analyzed by ID-TIMS: (1) the first fraction (50 ug) comprises short prismatic, light yellow, translucent euhedral crystals, some of which are broken, (2) the second and third fractions are made up of long columnar euhedral crystals, which are smaller than those of first fraction. Whereas the second fraction (25 ug) comprises transparent grains. Those from the third fraction (35 ug) are translucent (table 2). Zircons from the first fraction yield a $^{206}Pb/^{238}U$ apparent age of 293 ± 3 Ma. The second and third fraction zircons

TABLE 2

Zircon U-Pb isotopic analytical data of Aweitan and Adenbluk plutons (TIMS)

Fraction	Zircon characters	Weight (ug)	U (ug/g)	Pb (ug/g)	^{206}Pb (ng)	Ratio							Age (Ma)		
						$\frac{^{206}Pb}{^{204}Pb}$	$\frac{^{206}Pb}{^{238}U}$	±	$\frac{^{207}Pb}{^{235}U}$	±	$\frac{^{207}Pb}{^{206}Pb}$	±	$\frac{^{206}Pb}{^{238}U}$	$\frac{^{207}Pb}{^{235}U}$	$\frac{^{207}Pb}{^{206}Pb}$
Aweitan granite (A3) (Point 1, $^{206}Pb/^{238}U$ age 295±5Ma; point 2and point 3 weight $^{206}Pb/^{238}U$age 271±2Ma)															
1	Short prismatic, light yellow, transparent, euhedral, small	30	366	17	0.005	6335	0.04705	0.00072	0.3351	0.0072	0.05165	0.00071	296.4	293.4	269.2
2	Short prismatic, light yellow, transparent euhedral, big	30	279	12	0.001	25322	0.04314	0.00050	0.3031	0.0049	0.05096	0.00052	272.3	268.8	238.2
3	Long prismatic, light yellow, transparent, euhedral, big	35	453	23	0.15	314	0.04289	0.00043	0.3018	0.0048	0.05104	0.00008	270.7	267.8	242.6
Adenbluk monzogranite(A4)(Point 1, $^{206}Pb/^{238}U$ age 293±3Ma; point 2and point 3 weight $^{206}Pb/^{238}U$ age 271±5 Ma)															
1	Short prismatic, light yellow, translucent euhedral, big	50	127	6	0.008	2420	0.04642	0.00040	0.3343	0.0040	0.05223	0.0040	292.5	292.8	295.6
2	Long prismatic, light yellow transparent, euhedral, small	25	139	6	0.007	1368	0.04337	0.00107	0.3019	0.0110	0.0525	0.00125	273.7	267.9	217.9
3	Long prismatic, light yellow, translucent, euhedral, small	35	102	4	0.004	2561	0.04272	0.00104	0.2935	0.0108	0.04984	0.00126	269.6	261.3	187.4

TABLE 3

Chemical composition of the Permian granitoids in the Chinese Altai (wt. %, ppm)

Pluton	Buerjin				Xibodu				Daqiaonan		Aweitan	Adenbluk
Sample	97-1	3198	3199	3201	3055	3056	3061	3067	151	152	A4	A3
Rock	Monzogranite				Monzogranite				Granite		Granite	Monzogranite
Major Oxides												
SiO_2	75.12	69.45	69.20	69.34	72.19	71.49	73.63	72.60	69.15	70.03	67.41	67.79
TiO_2	0.23	0.44	0.43	0.42	0.30	0.30	0.43	0.14	0.58	0.62	0.41	0.64
Al_2O_3	13.12	14.87	15.08	15.07	14.16	14.33	13.02	14.41	14.64	14.55	15.41	15.80
Fe_2O_3T	1.85	2.77	2.80	2.76	1.78	1.80	2.71	1.06	3.71	3.67	2.88	4.32
MnO	0.06	0.05	0.06	0.06	0.05	0.05	0.04	0.03	0.06	0.07	0.10	0.13
MgO	0.40	1.10	1.08	1.07	0.52	0.51	0.69	0.20	0.96	0.93	0.49	1.71
CaO	1.38	2.18	2.25	2.24	1.27	1.26	1.41	0.68	1.79	1.79	1.18	2.64
Na_2O	3.25	3.75	3.59	3.58	3.77	3.83	3.06	3.86	3.60	3.67	5.20	4.38
K_2O	4.44	4.03	4.25	4.23	5.33	5.41	5.01	6.18	4.27	4.25	5.24	2.00
P_2O_5	0.07	0.18	0.18	0.18	0.08	0.08	0.14	0.03	0.34	0.37	0.10	0.10
LOI	0.50	0.82	0.90	0.90	0.64	0.80	0.78	0.70	0.56	0.48	1.85	1.14
Total	100.42	99.64	99.82	99.85	99.57	99.86	100.88	99.89	99.66	100.43	100.27	100.65
K_2O/Na_2O	1.37	1.07	1.18	1.18	1.41	1.41	1.64	1.60	1.19	1.16	1.01	0.46
A/CNK	1.15	1.19	1.20	1.21	1.15	1.08	1.17	1.06	1.20	1.19	1.01	1.34
A/NK	1.29	1.41	1.44	1.44	1.60	1.18	1.55	1.11	1.39	1.37	1.08	1.69
Trace element												
La	28.41	28.59	26.70	27.30	55.40	49.50	71.40	34.10	60.35	51.82	54.32	83.80
Ce	59.36	65.16	66.50	67.90	92.10	92.10	151.00	63.80	133.00	113.29	112.80	164.20
Pr	5.97	7.48	6.91	6.95	9.37	9.19	15.50	6.41	16.35	14.10	12.41	17.24
Nd	24.53	27.22	24.40	26.30	28.50	29.20	53.00	20.90	64.73	55.72	50.87	71.90
Sm	5.32	5.01	4.88	4.95	4.93	4.08	9.55	3.75	13.13	11.92	9.62	13.33
Eu	0.78	0.75	0.70	0.71	0.85	0.79	1.57	0.60	2.22	2.20	1.19	1.91
Gd	5.33	4.18	3.70	3.95	3.23	3.20	7.19	3.11	12.44	11.19	9.65	12.59
Tb	0.73	0.63	0.59	0.60	0.58	0.52	1.07	0.50	2.11	1.96	1.33	1.40
Dy	4.82	3.33	3.27	3.26	3.40	3.07	5.94	3.33	12.22	11.25	7.36	6.52
Ho	0.77	0.64	0.60	0.64	0.71	0.70	1.12	0.65	2.67	2.33	1.21	0.94
Er	2.32	1.81	1.74	1.76	2.16	1.93	3.13	1.93	6.84	5.86	3.23	2.42
Tm	0.30	0.29	0.26	0.28	0.34	0.29	0.41	0.32	1.02	0.88	0.43	0.33
Yb	1.90	1.91	1.58	1.68	2.26	2.03	2.65	2.10	6.68	5.77	2.67	1.60
Lu	0.31	0.29	0.26	0.27	0.35	0.31	0.41	0.32	1.04	0.89	0.42	0.27
Ba	145.30	444.10	427.00	442.00	405.00	446.00	438.00	753.00	493.22	534.87	428.30	93.46
Rb	190.00	177.34	194.50	199.30	119.00	131.70	94.90	201.80	134.38	172.56	93.00	122.00
Sr	107.10	283.45	298.90	305.50	231.00	249.80	150.00	220.90	146.97	149.07	121.40	139.20
Y	18.06	17.70	17.70	18.40	18.10	19.90	25.70	19.20	69.84	60.88	26.21	19.21
Zr	158.44	156.76	141.90	149.30	179.00	177.50	233.00	106.60	400.62	372.80	29.77	38.93
Nb	8.10	11.77	11.10	12.00	16.90	15.10	7.56	12.20	17.66	20.02	21.00	13.00

gave similar $^{206}Pb/^{238}U$ apparent ages with a weighted mean age of 271 ± 5 Ma (solid error ellipses in fig. 4D). The ages are similar as that of the Aweitan (fig. 4D), and the younger age agrees very well with the 273 ± 6 Ma age of the nearby Bielakuduke pluton (Han and others, 2006) and is interpreted as crystallization age of the Adenbluk pluton.

Whole Rock Elemental Geochemistry

The chemical compositions of the granitoids are given in table 3. Broadly, the rocks have "normal" SiO_2 (67-75%), low MgO (0.4-1.7%), high-K calc-alkaline characteristics (fig. 5A) with K_2O/Na_2O ratios generally >1 (fig. 5B). They are metaluminous to peraluminous based on their A/CNK values [= molar $Al_2O_3/(CaO+Na_2O+K_2O)$] that vary between 1.01 to 1.34 (fig. 5C). In terms of REE distribution, all the samples

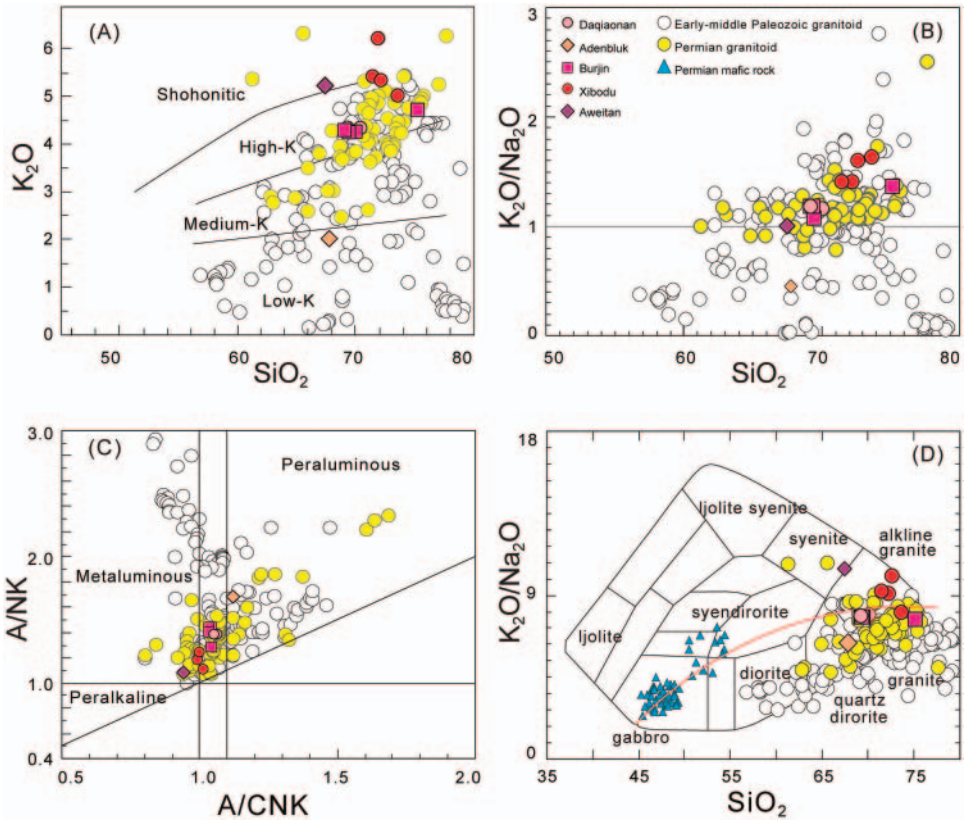

Fig. 5. Chemical classification diagrams for the Permian granitoids of the Chinese Altai: (A) SiO_2 vs. K_2O diagram (after Le Maitre and others, 1989). (B) SiO_2 vs. K_2O/Na_2O diagram. (C) A/CNK vs. A/NK diagram (after Maniar and Piccoli, 1989). (D) SiO_2 vs. K_2O/Na_2O diagram. Data sources include (1) Permian granitoids: Wang and others (2005), Tong and others (2006a, 2006b), Zhou and others (2007a, 2007b, 2009), Gong and others (2007), Gao and others (2010), Zhang and others (2010b, 2012), and Li and others (2012); (2) early-middle Palaeozoic granitoids: Wang and others (2006, 2009a), Yuan and others (2007), Liu and others (2012), and references therein; (3) Permian mafic intrusions: Chen and Han (2006), Li and others (2010), Gao and Zhou (2013a, 2013b), and references therein.

have typical "granitic" patterns with enrichment in LREE (La_N/Yb_N = 9-11.5) and distinct negative Eu anomalies (Eu/Eu* = 0.45-0.67) (fig. 6A). On the primitive-mantle normalized spider diagram, the rocks are enriched in large ion lithophile elements (LILEs, Cs, Rb, Th and K) and strongly depleted in high field strength elements (HFSEs, Ta, Nb, P, Ti) (fig. 6B), a feature commonly observed in highly differentiated granitic rocks.

Whole Rock Sr-Nd Isotopes

The Sr and Nd isotopic data for the Permian granitoids are given in table 4. Initial $^{87}Sr/^{86}Sr$ ratios and $\varepsilon_{Nd}(t)$ values were calculated back to the formation age of given plutons (zircon U-Pb age). The initial Sr isotopic ratios (I_{Sr}) show a large variation (0.7038-0.7104). It should be noted that I_{Sr} values calculated for high Rb/Sr rocks with highly radiogenic Sr isotopic compositions bear large uncertainties. All $\varepsilon_{Nd}(t)$ values of the Permian granitoids, including published data, are positive (+1.3 to +7.2) (table 4). The corresponding one-stage model ages (T_{DM1}) range from 1.3 to 0.5 Ga (table 4), most of them are younger than 0.9 Ga.

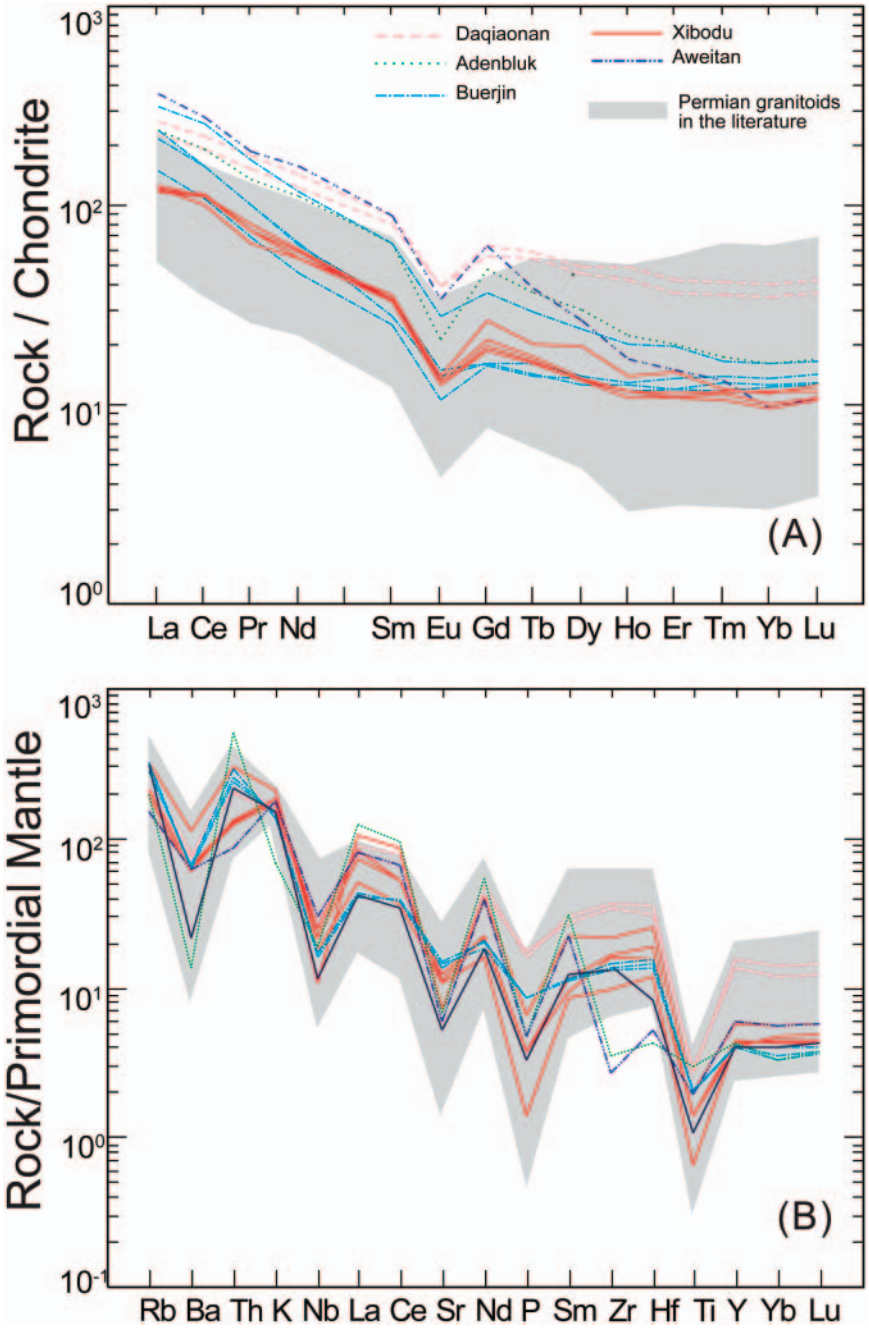

Fig. 6. Chondrite-normalized REE patterns and primitive-mantle normalized spidergrams for the Permian granitoids. The chondrite and primitive mantle values used for normalization in this work are from Sun and McDonough (1989). Data sources are same as figure 5.

TABLE 4

Sr, Nd isotopic data of Permian granitoids in the Chinese Altai

Sample	Pluton	Rock	Age (Ma)	Rb	Sr	$\frac{^{87}Rb}{^{86}Sr}$	$\frac{^{87}Sr}{^{86}Sr}$	2 σ	$\left(\frac{^{87}Sr}{^{86}Sr}\right)_i$	Sm	Nd	$\frac{^{147}Sm}{^{144}Nd}$	$\frac{^{143}Nd}{^{144}Nd}$	2σ	$f_{Sm/Nd}$	$\varepsilon_{Nd}(0)$	$\varepsilon_{Nd}(t)$	T_{DM1} (Ma)	T_{DM2} (Ma)	Data Source
151	Daqiaonan	Monzogranite	267	147.91	147.21	2.91	0.719123	18	0.7077	20.08	102.09	0.1189	0.512614	15	-0.40	-0.5	2.2	864	871	
152	Daqiaonan	Monzogranite	267	164.90	147.73	3.23	0.720604	25	0.7080	17.75	82.67	0.1298	0.512586	12	-0.34	-1.0	1.3	1026	947	
A4	Aweitan	Monzogranite	271							2.87	17.49	0.0992	0.512744	9	-0.50	2.1	5.4	543	603	
A3	Adenbluk	Monzogranite	271							12.59	66.21	0.1059	0.512771	16	-0.46	2.6	5.7	538	578	
97-18	Adenbluk	Monzogranite	271							6.59	30.34	0.1315	0.512870	7	-0.33	4.5	6.8	522	491	
97-19	Adenbluk	Monzogranite	271							7.74	35.26	0.1327	0.512850	5	-0.33	4.1	6.4	567	527	
3055	Xibodu	Monzogranite	267	118.13	221.50	1.54	0.71067	11	0.7048	4.16	26.82	0.0936	0.512675	6	-0.52	0.7	4.2	605	700	
3098	Buerjin	Biotite monzogranite	268	265.16	177.80	1.93	0.71259	14	0.7053	4.78	24.38	0.1256	0.512733	12	-0.36	1.9	4.3	724	697	This paper
97-1	Buerjin	Biotite monzogranite	268							5.60	24.91	0.1361	0.512856	11	-0.31	4.3	6.3	580	527	
97-2	Buerjin	Biotite monzogranite	268							4.54	23.05	0.1192	0.512630	10	-0.39	-0.2	2.5	841	846	
A14	Fuyunnan	granodiorite	275							11.61	53.51	0.1312	0.512808	12	-0.33	3.3	5.6	633	545	
A13	Fuyunnan	Mylonited diorite	282							1.24	6.47	0.1154	0.512852	12	-0.41	4.2	7.1	463	476	
189-1	Fuyunnan	Mylonited diorite	282	8.9	562.87	0.05	0.70459	12	0.7044	1.21	6.20	0.1176	0.512808	14	-0.40	3.3	6.2	543	546	
190-1	Fuyunnan	Mylonited diorite	282	7.76	670.6	0.03	0.70447	10	0.7043	1.02	7.24	0.0855	0.512660	11	-0.57	0.4	4.4	583	782	
258	Lamazao	Monzogranite	276	173.6	125.47	4.01	0.72573	16	0.7100	7.09	28.17	0.1523	0.51263	12	-0.23	-0.2	1.4	1292	943	Wang and others, 2005
259/1	Lamazao	Monzogranite	276	236.2	118.6	5.77	0.72734	2	0.7047	6.21	30.01	0.1252	0.512655	18	-0.36	0.3	2.9	855	823	Wang and others, 2005
K-1	Lamazao	Monzogranite	276	142.51	122.23	3.38	0.723664		0.7104	6.46	31.94	0.1223	0.512586	0.5	-0.38	-1.0	1.6	941	899	Wang and others, 1993
380105	Takeshiken	syenite	286	46.79	298	0.45	0.70585	10	0.7040	8.72	43.93	0.12	0.512816	5	-0.39	3.5	6.3	546	546	Tong and others, 2006b
380101-2	Takeshiken	Quartz syenite	286	91.8	122.1	2.18	0.71266	11	0.7038	7.76	40.38	0.1162	0.512805	6	-0.41	3.3	6.2	542	552	Tong and others, 2006b
380102-1	Takeshiken	Mafic enclave	286	8.17	532.4	0.04	0.70466	10	0.7045	2.24	8.18	0.1656	0.512949	9	-0.16	6.1	7.2	640	468	Tong and others, 2006b

Note: $\varepsilon_{Nd} = ((^{143}Nd/^{144}Nd)_s/(^{143}Nd/^{144}Nd)_{CHUR} - 1) \times 10000$, $f_{Sm/Nd} = (^{147}Sm/^{144}Nd)_s/(^{147}Sm/^{144}Nd)_{CHUR} - 1$, where s = sample, $(^{143}Nd/^{144}Nd)_{CHUR} = 0.512638$, and $(^{147}Sm/^{144}Nd)_{CHUR} = 0.1967$. The model ages ($T_{DM}$) were calculated using a linear isotopic ratio growth equation: $T_{DM} = 1/\lambda x \ln(1 + ((^{143}Nd/^{144}Nd)_s - 0.51315)/((^{147}Sm/^{144}Nd)_s - 0.2137))$. The two-stage model age is obtained assuming that the protolith of the granitic magmas has a Sm/Nd ratio (or $f_{Sm/Nd}$ value) of the average continental crust (Keto and Jacobsen, 1987). The $T_{DM-2} = (T_{DM1} - (T_{DM1} - t)(fcc - fdm))/(fcc - fdm)$, where fcc, fs, fdm = $f_{Sm/Nd}$ values of the average continental crust, the sample and the depleted mantle, respectively. fcc = 0.4, fdm = 0.08592, t = the intrusive age of granite.

Zircon Hf Isotopes

The zircon Hf isotopic compositions for three Permian plutons (Buerjin, Xibodu and Daqiaonan) are presented in table 5. The Xibodu pluton has highly positive $\varepsilon_{Hf}(t)$ values (+10.0 to +12.9) and young Hf T_{DM} model ages (537-397 Ma). The Daqiaonan pluton also has positive $\varepsilon_{Hf}(t)$ values (+6.1 to +8.0), only slightly lower than the Xibodu pluton and somewhat older model ages (668-554 Ma). The Buerjin pluton has a more variable zircon Hf isotope composition with $\varepsilon_{Hf}(t)$ values from +5.6 to +12.9 and T_{DM} model ages from 710 to 511 Ma.

DISCUSSION

Spatial and Temporal Distribution of the Permian Intrusions

Granitoids and granitic gneisses occupy *ca.* 70 percent of the surface exposures of the Chinese Altai (Windley and others, 2002). In the past few years, more than 100 zircon U-Pb ages were obtained, and the new data demonstrated that most plutons are older and were generated already during the early-middle Paleozoic (fig. 7, Wang and others, 2006; Yuan and others, 2007; Tong and others, 2007; Cai and others, 2011b; Yang and others, 2011a), especially highly deformed plutons (fig. 1). Meanwhile, Permian plutons become of great interest in terms of understanding their frequency and distribution in this orogen.

Our new U-Pb zircon ages (268±5 Ma, 267±6 Ma, 267±5 Ma, 271±2 Ma, and 271±5 Ma) of the Buerjin, Xibodu, Daqiaonan, Aweitan, and Adenbluk granitic plutons reveal that these rocks formed in a short time interval between 271 and 267 Ma Additionally, previous U-Pb zircon age investigations on the Lamazhao granite (276 ± 9 Ma, Wang and others, 2005), Fuyunnan deformed granite (282 ± 2 Ma) and undeformed granite (275 ± 2 Ma) (Tong and others, 2006a), Takeshiken syenite granite (286 ± 4 Ma, Tong and others, 2006b), Mayin'ebo granite (283 ± 4 Ma, Zhou and others, 2007a) and Fuyun gneissic granite (283 ± 4 Ma, Zhang and others, 2012), gave only slightly older ages. We have compiled all the available zircon U-Pb age data from our new analyses and the literature source, and the result appears that more than twenty Permian granitic plutons occur in the Chinese Altai (fig. 1). They mostly emplaced during 290 to 270 Ma with a peak age of ~278 Ma (fig. 8), roughly coeval with the activity of the Tarim plume (Zhang and others, 2010a, 2010b; Li and others, 2011). It is slightly different from the felsic plutons in the south neighboring West Junggar and East Junggar. Most plutons in the West Junggar emplaced before 290 Ma with a ~305 Ma A-type granite accumulation. In the East Junggar, alkali granites heavily over represent, but few of them formed during 285 to 250 Ma.

Finally, most Permian plutons or dikes occur in the south unit of the Chinese Altai and few are located in the central part (figs. 1 and 8), most of which are distributed along major NW-SW trending faults at the southern Chinese Altai; whereas the early-middle Paleozoic granitoids are widely distributed throughout the Chinese Altai (fig. 1). The different distribution indicates that the Permian plutons may have different origin and tectonic settings from that of early-middle Paleozoic granitoids.

Origin and Sources of the Permian Granitoids

Although Permian granitoids in the Chinese Altai have high K_2O, they have relatively low Zr+Nb+Y+Ce and 10000×Ga/Al ratios and show highly fractionated geochemistry, suggesting that they are highly fractionated I-type granite rather than A-type granite. These granitoids have highly positive $\varepsilon_{Nd}(t)$ (+1.3 to +7.2) and $\varepsilon_{Hf}(t)$ (+5.6 to +12.9) values, indicating a dominant proportion of isotopically depleted source in the magma genesis (tables 4 and 5). These rocks generally exhibit enrichment of LREE and negative Eu anomalies (fig. 6A). In the spider diagram, they are strongly depleted in Ba, Sr, P and Ti (fig. 6B). These geochemical features could be

TABLE 5

Zircon Hf isotope analyses for the Permian granitoids in the Chinese Altai

Spot No.	$^{176}Yb/^{177}Hf$	$^{176}Yb/^{178}Hf$	$^{176}Hf/^{177}Hf$	2σ	$t_{U\text{-}Pb}$ (Ma)	$f_{Lu/Hf}$	$\varepsilon_{Hf}(t)$	T_{DM} (Ma)	$T_{DM}C$ (Ma)	$(^{176}Hf/^{177}Hf)_i$	$(^{176}Hf/^{177}Hf)_{(DM)i}$
Buerjin monzogranite (3198)											
1	0.035234	0.000628	0.282838	0.000027	298	-0.98	8.8	582	758	0.282835	0.283036
2	0.077304	0.001590	0.282854	0.000028	299	-0.95	9.2	574	733	0.282845	0.283035
3	0.059606	0.001179	0.282799	0.000022	295	-0.96	7.2	646	855	0.282792	0.283038
4	0.070730	0.001404	0.282837	0.000027	295	-0.96	8.5	595	772	0.282829	0.283038
5	0.082105	0.001603	0.282854	0.000027	274	-0.95	8.6	574	747	0.282846	0.283053
6	0.060172	0.001165	0.282796	0.000027	272	-0.96	6.6	650	875	0.282790	0.283055
7	0.083175	0.001610	0.282863	0.000024	269	-0.95	8.8	561	730	0.282855	0.283057
8	0.089811	0.001692	0.282774	0.000032	268	-0.95	5.7	691	933	0.282766	0.283058
9	0.059606	0.001179	0.282799	0.000022	263	-0.96	6.5	646	874	0.282793	0.283061
10	0.077959	0.001583	0.282759	0.000026	290	-0.95	5.6	710	953	0.282750	0.283042
11	0.080015	0.001717	0.282825	0.000029	273	-0.95	7.6	618	815	0.282816	0.283054
12	0.052228	0.001134	0.282824	0.000023	260	-0.97	7.4	609	818	0.282818	0.283063
13	0.041943	0.000915	0.282834	0.000025	268	-0.97	7.9	592	788	0.282829	0.283058
14	0.058929	0.001267	0.282822	0.000024	263	-0.96	7.3	614	822	0.282816	0.283061
15	0.073606	0.001558	0.282844	0.000023	295	-0.95	8.7	588	758	0.282835	0.283038
16	0.085921	0.001865	0.282900	0.000023	270	-0.94	10.1	511	648	0.282891	0.283056
17	0.084106	0.001998	0.282862	0.000022	294	-0.94	9.3	568	723	0.282851	0.283039
Xibodu monzogranite (3055)											
1	0.088583	0.002149	0.282949	0.000018	294	-0.94	12.3	443	527	0.282937	0.283039
2	0.073017	0.001843	0.282882	0.000024	295	-0.94	10.0	537	675	0.282872	0.283038
3	0.065232	0.001713	0.282900	0.000019	263	-0.95	10.0	509	650	0.282892	0.283061
4	0.092349	0.002267	0.282889	0.000023	298	-0.93	10.2	533	663	0.282876	0.283036
5	0.086220	0.001913	0.282979	0.000019	268	-0.94	12.9	397	470	0.282969	0.283058
6	0.111680	0.002303	0.282979	0.000023	271	-0.93	12.9	401	472	0.282967	0.283055
7	0.048149	0.001253	0.282917	0.000023	290	-0.96	11.3	479	591	0.282910	0.283042
8	0.058096	0.001254	0.282915	0.000024	290	-0.96	11.2	481	595	0.282908	0.283042
9	0.078909	0.001638	0.282925	0.000022	299	-0.95	11.7	472	572	0.282916	0.283035
10	0.049606	0.001128	0.282893	0.000025	295	-0.97	10.5	511	641	0.282887	0.283038
11	0.053103	0.001201	0.282884	0.000025	298	-0.96	10.3	525	660	0.282877	0.283036
12	0.065820	0.001637	0.282888	0.000021	295	-0.95	10.3	525	659	0.282879	0.283038
Daqiaonan Biotite granite (152)											
1	0.063255	0.001271	0.282783	0.000020	270.6	-0.96	6.1	670	906	0.282777	0.283056
2	0.077841	0.001531	0.282792	0.000019	264.6	-0.95	6.3	662	892	0.282784	0.283060
3	0.060156	0.001185	0.282819	0.000023	268.5	-0.96	7.4	617	825	0.282813	0.283057
4	0.063206	0.001256	0.282826	0.000021	264	-0.96	7.5	609	813	0.282820	0.283060
5	0.077679	0.001550	0.282798	0.000023	284.2	-0.95	6.9	654	868	0.282790	0.283046
6	0.083383	0.001722	0.282847	0.000018	258.6	-0.95	8.0	586	773	0.282839	0.283064
7	0.098848	0.002012	0.282794	0.000019	283	-0.94	6.6	668	883	0.282783	0.283047
8	0.099559	0.002181	0.282810	0.000019	265.5	-0.93	6.8	647	858	0.282799	0.283059
9	0.073883	0.001469	0.282838	0.000017	253.5	-0.96	7.7	595	794	0.282831	0.283068
10	0.068094	0.001384	0.282786	0.000018	267.3	-0.96	6.1	668	903	0.282779	0.283058
11	0.080230	0.001517	0.282819	0.000021	260.8	-0.95	7.1	623	833	0.282812	0.283063
12	0.088847	0.001708	0.282869	0.000028	244.1	-0.95	8.5	554	731	0.282861	0.283075

$\varepsilon_{Hf}(t) = 10{,}000 \times \{[(^{176}Hf/^{177}Hf)_S - (^{176}Lu/^{177}Hf)_S \times (e^{\lambda t} - 1)]/[(^{176}Hf/^{177}Hf)_{CHUR,0} - (^{176}Lu/^{177}Hf)_{CHUR} \times (e^{\lambda t} - 1)] - 1\}$. $T_{DM} = 1/\lambda - \ln\{1 + [(^{176}Hf/^{177}Hf)_S - (^{176}Hf/^{177}Hf)_{DM}]/[(^{176}Lu/^{177}Hf)_S - (^{176}Lu/^{177}Hf)_{DM}]\}$. $f_{Lu/Hf} = (^{176}Lu/^{177}Hf)_S/(^{176}Lu/^{177}Hf)_{CHUR} - 1$. Where, $\lambda = 1.867 \times 10^{-11}$ year^{-1} (Soderlund and others, 2004); $(^{176}Lu/^{177}Hf)_S$ and $(^{176}Hf/^{177}Hf)_S$ are the measured values of the samples; $(^{176}Lu/^{177}Hf)_{CHUR} = 0.0332$ and $(^{176}Hf/^{177}Hf)_{CHUR,0} = 0.282772$ (Blichert-Toft and Albarede, 1997); $(^{176}Lu/^{177}Hf)_{DM} = 0.0384$ and $(^{176}Hf/^{177}Hf)_{DM} = 0.28325$ (Griffin and others, 2002); $(^{176}Lu/^{177}Hf)_{mean\ crust} = 0.015$; $f_s = f_{Lu/Hf}$; $f_{DM} = [(^{176}Lu/^{177}Hf)_{DM}/(^{176}Lu/^{177}Hf)_{CHUR}] - 1$; t = crystallization time of zircon.

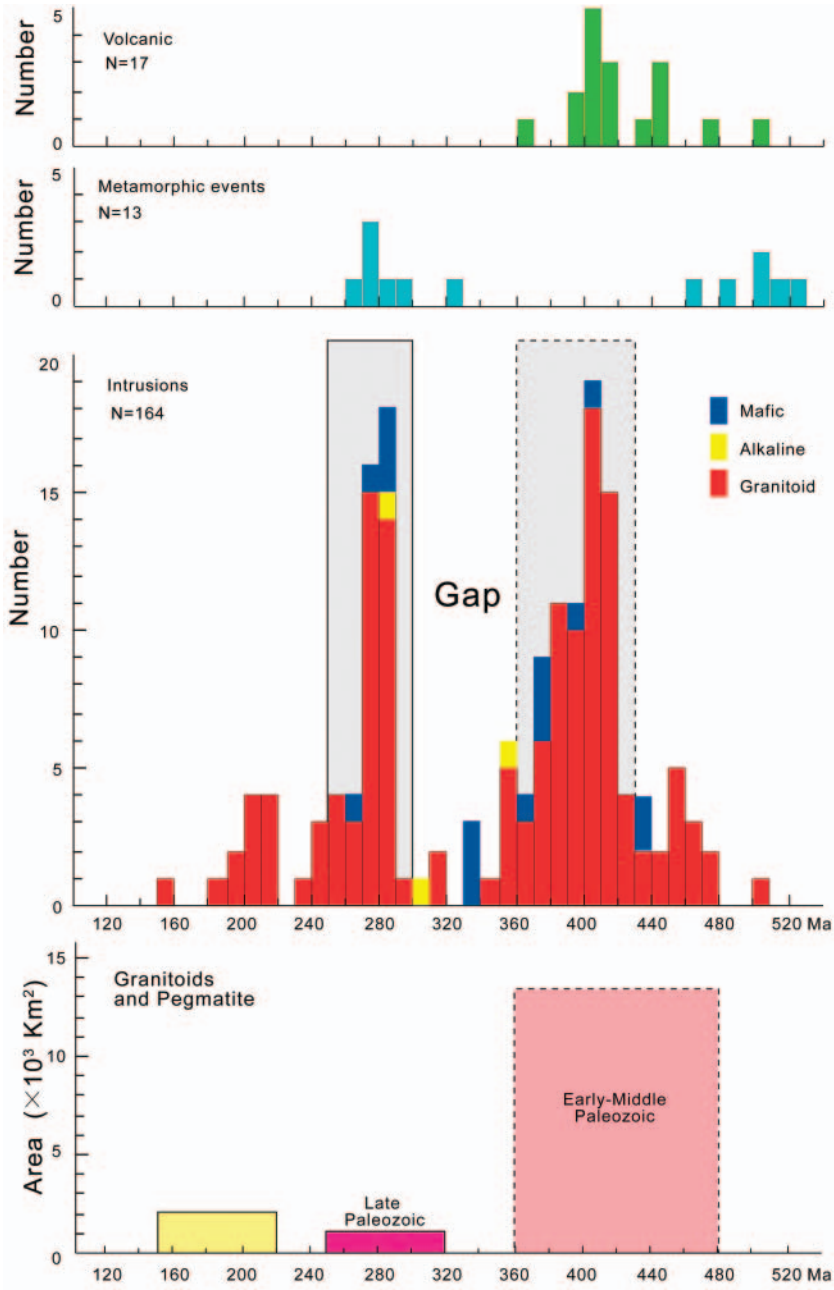

Fig. 7. Age histogram of the igneous rocks and distribution area statistic diagram of the granitoids in the Chinese Altai. The volcanic eruption age data are from Zhang and others (2000), and Chai and others (2008, 2009). The early-middle intrusions age data are from Wang and others (2006), Yuan and others (2007), Tong and others (2007), Cai and others (2011b, 2012), Yang and others (2011a), Liu and others (2012), Zhang and others (2012) and reference therein). Permian intrusions age data are given in table 6 and fig. 1. Most igneous rocks were emplaced in the early-middle Paleozoic and an apparent magmatism gap existed between early-middle Paleozoic and Permian. The areal extent of the Permian granitoids is smaller than that of the early-middle Paleozoic granitoids, probably indicating a weaker magma activity in the Permian.

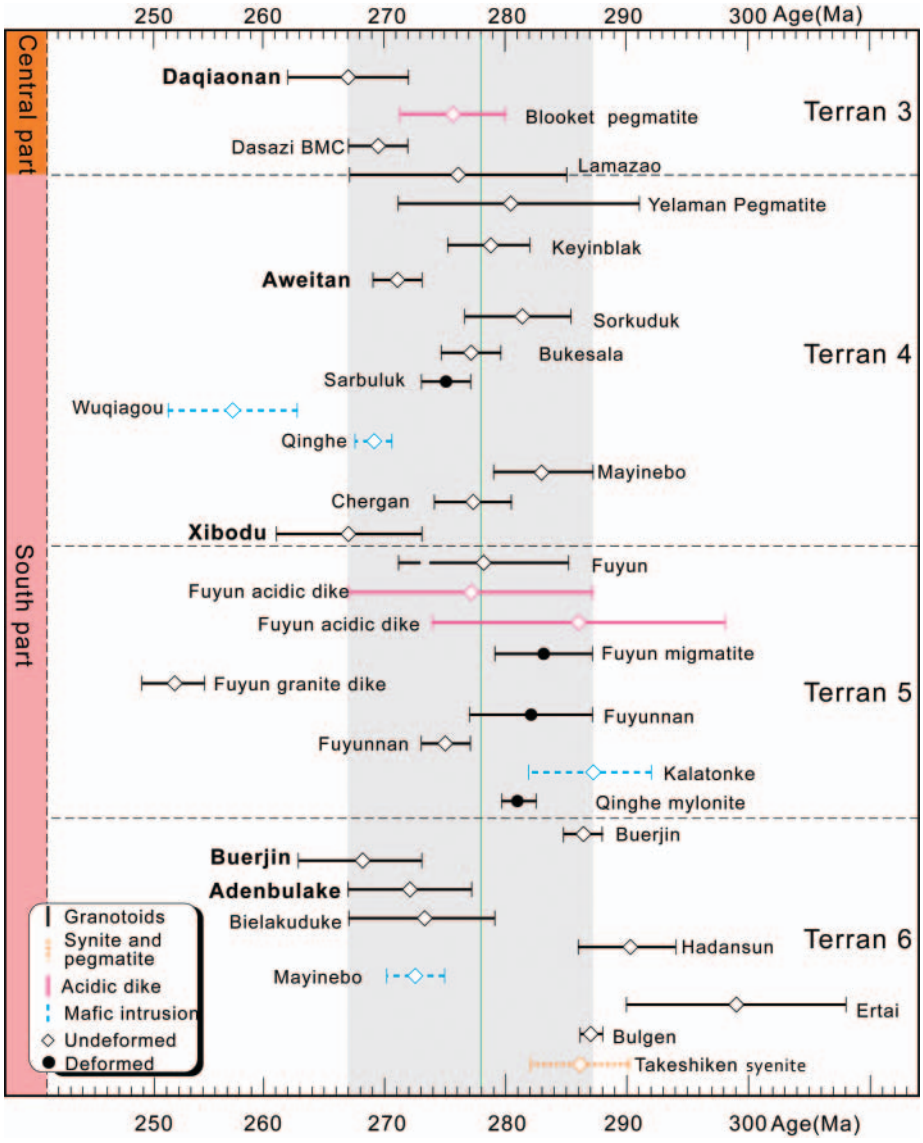

Fig. 8. Temporal and spatial distribution of the Permian intrusions from the Chinese Altai. Plutons are arranged from west to east in each terrane. Most plutons were emplaced during 287–267 Ma with a peak at ~278 Ma. They occur widely in the southern part of the orogen and only few in the central part.

produced by partial melting of either juvenile lower crust or mantle (Turner and others, 1992).

These rocks have very low Ni contents (1.0-10.3 ppm), possibly indicative of partial melting of crustal rocks. However, partial melting of juvenile basaltic lower crust would likely produce sodium-rich magmas rather than high-K melts (Atherton and Petford, 1993). Most Permian granitoids have high-K calc-alkaline composition with high K_2O/Na_2O ratios (1.01-1.64 except the monzogranite with 0.46), and sufficiently differ from early-middle Paleozoic granitoids (fig. 5), which does not support the idea of

partial melting of juvenile lower crust as early-middle Paleozoic granitoids (Wang and others, 2006, 2009a; Yuan and others, 2007; Liu and others, 2012). This is also supported by the Nd and Hf isotopic compositions (fig. 9). On the other hand, Permian granitoids compose a magma association with more felsic and coeval mafic intrusions (fig. 5D) (Han and others, 2004; Zhang and others, 2012; Gao and Zhou, 2013a). Therefore, mantle-derived magma may have played an important role in the formation of Permian granitoids in the Chinese Altai. These Permian rocks have highly variable Nd (+1.3 to +7.2) and Hf (+5.6 to +12.9) isotopic compositions (fig. 9). They also have highly variable elemental compositions, particularly REE contents and patterns. Such different isotopic and elemental compositions are indicative of heterogeneous mantle sources or addition of crustal material into mantle-derived magmas (Blichert-Toft and Albarède, 1997). Most of the granitoids have inherited zircons, indicating the addition of crustal materials. Thus, these Permian granitoids may have formed by fractionation of mantle-derived magmas combined by crustal contamination.

It was suggested that the Permian granitic plutons were generated in an extensively extensional continental environment. Upwelling of the hot asthenospheric mantle and/or decompression might have triggered the partial melting of the mantle source underneath the Chinese Altai to produce parental magmas that have formed these Permian granitoids and the Erqis strike-slip Fault may have acted as major channel for melt propagation (Buslov, 2011).

Permian Post-collisional Setting

The Permian tectonic setting in the Altai orogen is still debated. Some researchers suggested that the accretionary orogenic process lasted until the late Carboniferous to Permian (Cai and others, 2012) and that active continental margins still existed in the Chinese Altai during the early Permian (Hu and others, 2006; Chen and others, 2006; Xiao and others, 2008). In other research work, it was argued that the geodynamic setting changed into a post-orogenic or post-collisional extensional environment during the late Paleozoic (Wang and others, 2010; Tong and others, 2012), especially in the Permian (Wang and others, 2005; Tong and others, 2006b; Briggs and others, 2007, 2009; Zhou and others, 2007a, 2007b, 2009; Zhang and others, 2012). In the following we present several lines of evidence to argue for a post-collisional or post-accretionary setting for the Permian magmatism.

(1) Evidence from structural patterns

Most Permian granitic plutons in the Chinese Altai are approximately circular, with essentially no solid stage deformational fabric, and commonly cross-cutting the previous tectonic lineament and structural features (for example, the regional foliations). This is displayed in the Adenbluk (fig. 2B), Lamazhao (fig. 2C) and Takeshiken plutons (fig. 2D, Tong and others, 2006b), and their circular shape is clearly visible in the satellite photos. Taking the Lamazhao pluton for example, this pluton displays an almost perfect round shape with no fabrics, and it intrudes the boundary of north unit and central unit (fig. 1 in Wang and others, 2005) and crosscuts the fault and regional structures like a "stitching" pluton (Han and others, 2010). In addition, the late Permian undeformed acidic dike swarm in the Fuyun area has a consistent direction perpendicular to the strike of the Erqis fault zone and regional structural lineament (Gong and others, 2007; Zhang and others, 2012). Thus, these observations constrain the timing of the regional deformation and the activity of the Erqis Fault. Except for the Erqis Fault strike-slip ductile deformation that was sustained until the late Permian in this area, there is no regional scale deformation during the Permian and later.

(2) Evidence from regional geology

The main regional ductile deformation/metamorphism in the Chinese Altai took place during the early-middle Paleozoic (Wang and others, 2006; Wei and others,

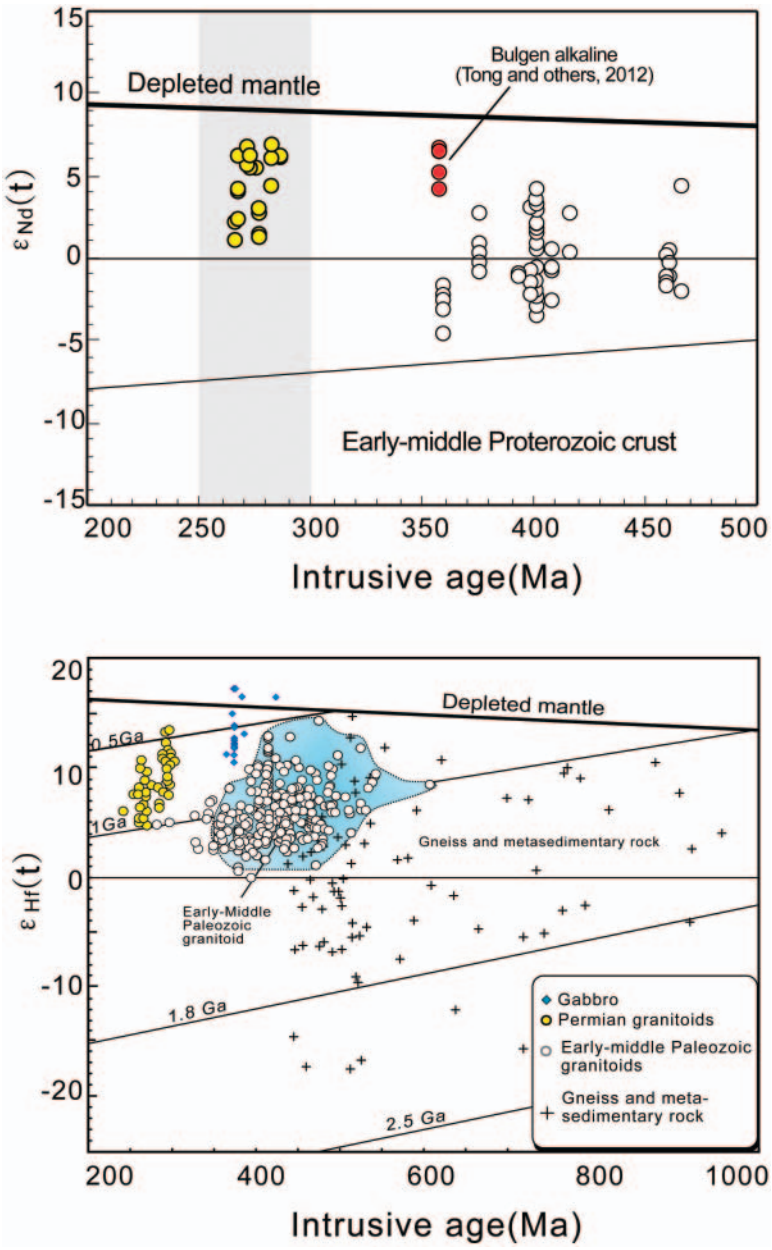

Fig. 9. $\varepsilon_{Nd}(t)$ vs. age (Ma) diagram for the granitoids and Zircon $\varepsilon_{Hf}(t)$ vs. age (Ma) diagram for plutonic rocks and gneisses from the Chinese Altai. Note that the $\varepsilon_{Nd}(t)$ values of the granites increase from early-middle Paleozoic to late Paleozoic (Data of Permian granitoids from table 5, others from Wang and others (2009), Liu and others (2012) and reference therein; signs as in fig. 5. The $\varepsilon_{Hf}(t)$ values of all granites are positive, suggesting an important role of the mantle-derived material in the generation of the Permian granitoids. [Data for Permian granitoids from table 4, others from Sun and others (2008, 2009), Cai and others (2011b), Liu and others (2012), and references therein].

2007), but little or none during the Permian (Wang and others, 2009b). It is interesting to note that Permian magmatism started after a phase of magmatic

TABLE 6

Summarized zircon U-Pb ages of the Permian granitoids and coeval rocks in the Chinese Altai orogen

Stage	Granitoids						Other rocks				
	Age(Ma)	Rock type	Terrane	Deformation	Reference	No. in fig.1	Age (Ma)	Rock type	Terrane	Reference	No. in fig.1
299 - 290 Ma	299 ± 9	Ertai granodiorite	6	N	Li and others, 2004	R					
							293 ± 4	Medium-to low-pressure pelitic granulite	4	Wang and others, 2009b	
	290 ± 4	Hadansun granite	6	N	Zhou and others, 2009	Q					
287 - 267 Ma	287	Bulgen K-feldspar granite	6	N	Liu and others, 1996	S	287 ± 5	Kelatongke gabbro	5	Han and others, 2004	N
	286 ± 4	Takeshiken synite granite	6	N	Tong and others, 2006b	T	286 ± 12	Fuyun acidic dike	5	Briggs and others, 2007	K
	286.3 ± 1.6	Buerjin granodiorite	6	N	Zhang and others, 2012	H					
	283 ± 4	Mayin'ebo peraluminous granite	4	*Y*	Zhou and others, 2007a	O	283 ± 4	Fuyun migmatite	5	Zhang and others, 2012	H
	282 ± 5	Fuyunnan deformed granite	5	*Y*	Tong and others, 2006a	L					
	281 ± 1.4	Qinghe granitic mylonite	5	*Y*	Zhou and others, 2007b	P	281 ± 3	Qinghe andesitic gneiss	5	Hu and others, 2006	
							281 ± 10	Yelaman pegmetite	4	Sun and others, 2009b	F
	280.9 ± 4.3	Sorkuduk biotite granite	4	N	Gao and others, 2010	B	281 ± 6	Altai gabbro	4	This paper	
	278.6 ± 3.5	Keyinblak	4	N	Li and others, 2012	G	279.0 ±5.6	Fuyun basic granulite	4	Chen and others, 2006	
							278 ± 7	Fuyun acidic dike		Briggs and others, 2007	K
	277.0 ± 2.4	Buksela biotite monzogranite	4	N	Gao and others, 2010	B	277 ± 10	Fuyunan diorite	5	Gong and others, 2007	J
	277.2 ± 3.2	Chergan granite	4	N	Zhang and others, 2010b	E					
	276 ± 9	Lamazao granite	4-5	N	Wang and others, 2005	A					
	275.7 ± 1.7	Shaerbulake tow-mica granite	4	*Y*	Sun and others, 2009a	C	275.5 ± 4.2	Blooket pegmatite	3	Ren and others, 2011	D
	275 ± 2	Fuyunnan granite	5	N	Tong and others, 2006a	L					
	273 ± 6	Bielakuduke granite	5	N	Han and others, 2006	I					
	271 ± 5	Adenbluk granite	6	N	This paper		272.5 ± 2.4	Mayinebo gabbro	6	Zhang and others, 2010b	E
	271 ± 2	Aweitan granite	4	N	This paper		271.0 ± 6.0	Fuyun basic granulite	4	Chen and others, 2006	
							271.0 ± 5.4	Fuyun basic granulite	4	Chen and others, 2006	
							269.4 ± 2.5	Dasazi bimodal complex	3	Zhang and others, 2010b	E
							269.0± 1.5	Qinghe gabbro	3	Zhang and others, 2012	H
	268 ± 5	Burjin granite	6	N	This paper		268.0 ± 5.5	Fuyun basic granulite	4	Chen and others, 2006	
	267 ± 6	Xibodu granite	5	N	This paper						
	267 ± 5	Daqiaonan granite	3	N	This paper						
257 - 252 Ma							257.4 ± 5.3	Wuqiagou mafic	4	Chen and Han, 2006	M
	252.4 ± 2.6	Fuyun granite dike	5	N	Zhang and others, 2012	H					

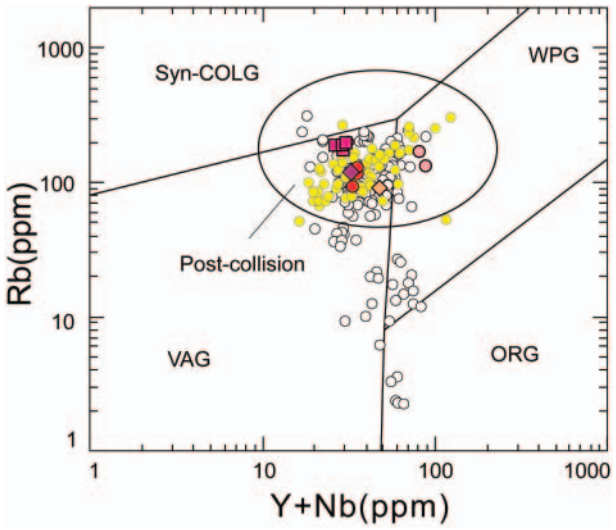

Fig. 10. Rb versus Y+Nb tectonic discrimination diagram (Pearce and others, 1984). (Signs as in fig. 5). Abbreviations: ORG — orogenic granites; syn-COLG — syn-collisional granites; VAG — volcanic arc granites; WPG — within plate granites.

quiescence (fig. 7). Amongst the Permian granites only those are deformed which are restricted to the vicinity of the Erqis fault zone (figs. 1 and 8 and table 6, Tong and others, 2006a; Sun and others, 2009a; Zhou and others, 2009). Incidentally, the Erqis fault zone underwent a sinistral strike-slip ductile deformation during 290 to 275 Ma (table 6, Travin and others, 2001; Buslov and others, 2004; Tong and others, 2006a; Zhou and others, 2007b; Briggs and others, 2007, 2009; Zhang and others, 2012) and thus, deformation of those granites is related to movement along this fault.

Moreover, ophiolitic rocks in the Chinese Altai and adjacent area are pre-Carboniferous in age (Li, 1995; Jian and others, 2003; Zhang and others, 2003; Xiao and others, 2004; Wong and others, 2010). Thus, they bear no evidence for the existence of a late Paleozoic (<350 Ma) ocean. Finally, the lack of Permian arc-related volcanic rocks and/or marine sediment in the Chinese Altai further argued against a subduction zone setting of this orogen during the Permian (fig. 7).

(3) Evidence from geochemical characterization

The Permian granitoids show geochemical features different from early-middle Paleozoic granitoids (Wang and others, 2005; Tong and others, 2006b; Li and others, 2012). The granites have high K_2O and low Al_2O_3 and are metaluminous to weakly peraluminous with concentrated A/NK and A/CNK values. In contrast, the early-middle Paleozoic granitoids and granodiorites have low K_2O but high Al_2O_3 with high A/NK ratios (figs. 4A and 4B). Permian granitoids have highly positive $\varepsilon_{Nd}(t)$ (+1.3 to +7.2) and $\varepsilon_{Hf}(t)$ (+5.6 to +12.9) values, also different from the Nd isotopic compositions of early-middle Paleozoic granitoids (−4.5 to +5.2, most <0) (fig. 9), which have higher proportions of ancient crustal source (Wang and others, 2006, 2009a; Yuan and others, 2007; Liu and others, 2012). In tectonic discrimination diagrams (Pearce and others, 1984), the early-middle granitoids plot in volcanic arc granite (VAG) field, whereas the Permian granitoids plot in the post-collisional field (fig. 10). These different compositional characteristics probably indicate an important change in the tectonic environment towards the end of the Paleozoic, such as, from a subduction/accretionary compressional environment to a post-accretionary extensional setting.

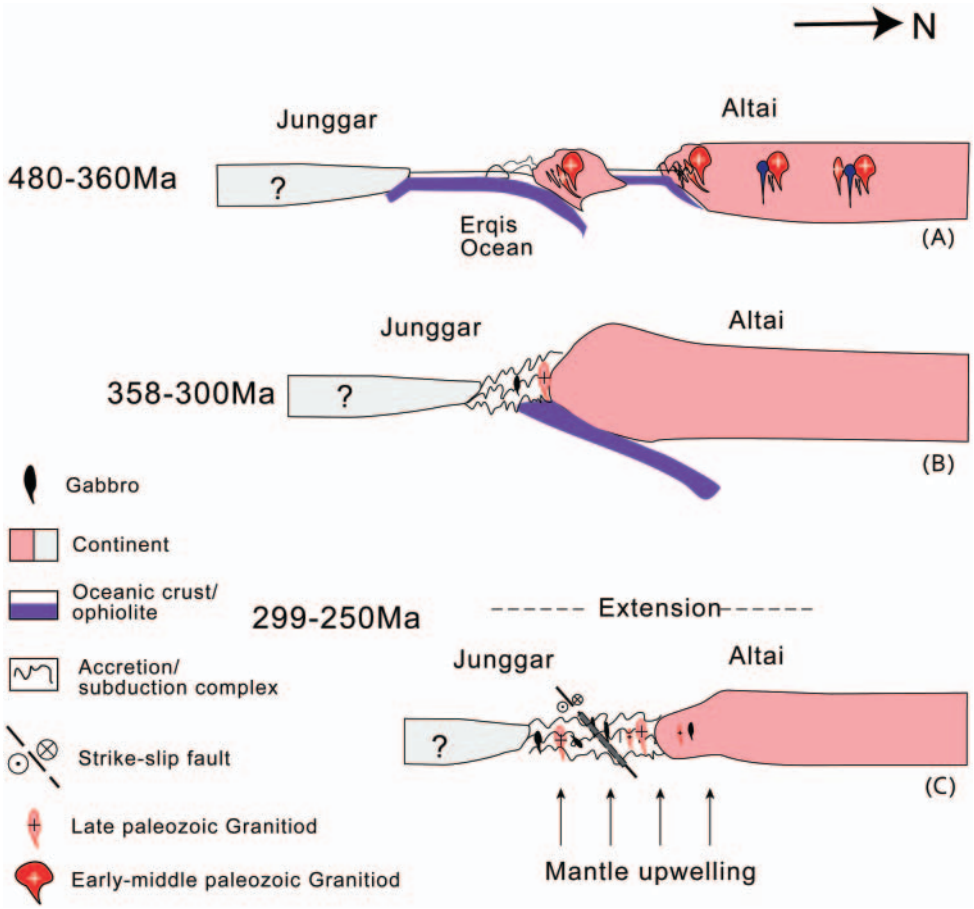

Fig. 11. A tectonic model showing middle-late Paleozoic evolution of the Chinese Altai (Modified from Wang and others, 2006; Tong and others, 2012). (A) The Erqis ocean subduction stage; (B) the Piece-transition stage; (C) the Permian post-collisional extension stage.

From the discussion above, it appears that the Erqis Ocean was completely closed before the Permian. The accretion of Altai orogen terminated and was already transformed into a post-collisional or post-accretionary setting after the collision and amalgamation of the Altai and Junggar blocks (fig. 11, Wang and others, 2010; Gao and Zhou, 2013a). Thus the Chinese Altai comprises a complete orogenic-magmatic cycle from subduction through continental-arc collision to post-collision.

Note that the crust of East and West Junggar was invaded by numerous A-type granitoids from later Carboniferous to early Permian (Liu and others, 1996; Han and others, 1997; Geng and others, 2009), indicative of a regional extensional environment. The occurrence of the late Carboniferous Sikeshu "stitching pluton" is evidence for a post-collisional setting of the North Tianshan in the Permian (Han and others, 2010). The magmatic, sedimentary or tectonic records in the Junggar Basin and its surroundings do not support the idea of subduction in the Permian (West and East Junggar, Altai, North Tianshan) (Buckman and Aitchison, 2004; Han and others, 2006, 2010; Yang and others, 2011b; Choulet and others, 2012). In any case, the whole northern Xinjiang was in a post-collisional extension setting during the Permian (Han

and others, 2010, 2012; Tong and others, 2010), concomitant with large-scale mantle-related Ni-Cu sulfide mineralization (Mao and others, 2006; Song and Li, 2009; Pirajno, 2010; Pirajno and others, 2011; Gao and others, 2012a,b; Gao and Zhou, 2013a,b). Furthermore, this observation is consistent with the occurrence of widespread and voluminous post collisional Permian intrusions in the entire CAOB. Except those along the southern margin of the CAOB (Jian and others, 2010), most granitoids in CAOB are post-collisional (Hong and others, 1994; Konopelko and others, 2007; Jahn and others, 2009; Han and others, 2011), and some that are near the Tarim Block might be related to the large igneous province in the Tarim Block (Li and others, 2011).

CONCLUSIONS

Five plutons from the Chinese Altai give zircon U-Pb ages between 271 and 267 Ma. Combined with previous radiometric ages, we can state that Permian granitic plutons in the Chinese Altai mainly emplaced during 287 to 267 Ma with a peak age of ~278 Ma. The granitoids have positive $\varepsilon_{Nd(t)}$ (+1.3 to +7.2) and $\varepsilon_{Hf(t)}$ (+5.1 to +12.9) suggest a contribution of mantle magma. Upwelling of the hot asthenospheric mantle after the collision and amalgamation of the Altai and Junggar blocks probably triggered partial melting of mantle source. From structural pattern, rock assemblages, whole-rock geochemical characteristics, magma evolution, and regional geology, it is concluded that the Permian intrusions were emplaced in a post-collisional or post-accretionary setting. This study provides evidence that Permian magmatism occurred widespread in the western part of the CAOB.

ACKNOWLEDGMENTS

This work was financially supported by the National Natural Science Foundation of China (NSFC grant 40702010), the Basic Outlay of Scientific Research Work from the Ministry of Science and Technology of the People's Republic of China (J0709, J0906, and J1116), China Geological Survey Project (1212011085474, 1212011309650) and a Hong Kong RGC grant (704712P). We gratefully acknowledge the careful and constructive comments of M. H. Ren, W. Siebel, F. K. Chen, and the two reviewers, which considerably improved the manuscript. We also thank Z. Q. Yan, H. Zhou, X. M. Liu for laboratory assistance. Bor-ming Jahn acknowledges the support of NSC-Taiwan through the following grants: NSC100-2116-M-002-024, NSC100-2923-M-002-010, NSC 101-2116-M-002-003, NSC 102-2923-M-002-009.

REFERENCES

Andersen, T., 2002, Correction of common lead in U-Pb analyses that do not report ^{204}Pb: Chemical Geology, v. 192, n. 1–2, p. 59–79, http://dx.doi.org/10.1016/S0009-2541(02)00195-X

Atherton, M. P., and Petford, N., 1993, Generation of sodium-rich magmas from newly underplated basaltic crust: Nature, v. 362, p. 144–146, http://dx.doi.org/10.1038/362144a0

Black, L. P., Kamo, S. L., Williams, I. S., Mundil, R., Davis, D. W., Korsch, R. J., and Foudoulis, C., 2003, The application of SHRIMP to Phanerozoic geochronology; a critical appraisal of four zircon standards: Chemical Geology, v. 200, n. 1–2, p. 171–188, http://dx.doi.org/10.1016/S0009-2541(03)00166-9

Blichert-Toft, J., and Albarède, F., 1997, The Lu-Hf geochemistry of the chondrites and the evolution of the mantle-crust system: Earth and Planetary Science Letters, v. 148, n. 1–2, p. 243–258, http://dx.doi.org/10.1016/S0012-821X(97)00040-X

Briggs, S. M., Yin, A., Manning, C. E., Chen, Z. L., Wang, X. F., and Grove, M., 2007, Late Paleozoic tectonic history of the Ertix Fault in the Chinese Altai and its implications for the development of the Central Asian Orogenic System: Geological Society of America Bulletin, v. 119, n. 7–8, p. 944–960, http://dx.doi.org/10.1130/B26044.1

Briggs, S. M., Yin, A., Manning, C. E., Chen, Z. L., and Wang, X. F., 2009, Tectonic development of the southern Chinese Altai Range as determined by structural geology, thermobarometry, ^{40}Ar/^{39}Ar thermochronology, and Th/Pb ion-microprobe monazite geochronology: Geological Society of America Bulletin, v. 121, n. 9–10, p. 1381–1393, http://dx.doi.org/10.1130/B26385.1

Buckman, S., and Aitchison, J. C., 2004, Tectonic evolution of Palaeozoic terranes in West Junggar, Xinjiang, NW China, *in* Malpas, J., Fletcher, C. J. N., Ali, J. R., and Aitchison, J. C., editors, Aspects of the Tectonic

Evolution of China: Geological Society, London, Special Publications, v. 226, p. 101–129, http://dx.doi.org/10.1144/GSL.SP.2004.226.01.06

Buslov, M. M., 2011, Tectonics and geodynamics of the Central Asian fold belt: the role of the Late Paleozoic large-amplitude strike-slip faults: Russian Geology and Geophysics, v. 52, n. 1, p. 52–71, http://dx.doi.org/10.1016/j.rgg.2010.12.005

Buslov, M. M., Watanabe, T., Fujiwara, Y., Iwata, K., Smirnova, L. V., Safonova, I. Y., Semakov, N. N., and Kiryanova, A. P., 2004, Late Paleozoic faults of the Altai region, Central Asia: tectonic pattern and model of formation: Journal of Asian Earth Sciences, v. 23, n. 5, p. 655–671, http://dx.doi.org/10.1016/S1367-9120(03)00131-7

Cai, K. D., Sun, M., Yuan, C., Zhao, G. C., Long, X. P., and Xiao, W. J., 2011a, Geological framework and Paleozoic tectonic history of the Chinese Altai, NW China: a review: Russian Geology and Geophysics, v. 52, n. 12, p. 1619–1633, http://dx.doi.org/10.1016/j.rgg.2011.11.014

Cai, K. D., Sun, M., Yuan, C., Zhao, G. C., Xiao, W. J., Long, X. P., and Wu, F. Y., 2011b, Prolonged magmatism, juvenile nature and tectonic evolution of the Chinese Altai, NW China: Evidence from zircon U-Pb and Hf isotopic study of Paleozoic granitoids: Journal of Asian Earth Sciences, v. 42, n. 5, p. 949–968, http://dx.doi.org/10.1016/j.jseaes.2010.11.020

Cai, K. D., Sun, M., Yuan, C., Zhao, G. C., Xiao, W. J., and Long, X. P., 2012, Keketuohai mafic-ultramafic complex in the Chinese Altai, NW China: Petrogenesis and geodynamic significance: Chemical Geology, v. 294–295, p. 26–41, http://dx.doi.org/10.1016/j.chemgeo.2011.11.031

Chai, F. M., Mao, J. W., Dong, L. H., Yang, F. Q., Liu, F., Geng, X. X., Yang, Z. X., and Huang, C. K., 2008, SHRIMP Zircon U-Pb Dating for metarhyolites of the Kangbutiebao Formation at the Abagong iron deposit in the southern margin of the Altay, Xinjiang and its geological Significance: Acta Geologica Sinica, v. 82, n. 11, p. 1592–1601 (in Chinese with English Abstract).

Chai, F. M., Mao, J. W., Dong, L. H., Yang, F. Q., Liu, F., Geng, X. X., and Zhang, Z. X., 2009, Geochronology of metarhyolites from the Kangbutiebao Formation in the Kelang basin, Altay Mountains, Xinjiang: Implications for the tectonic evolution and metallogeny: Gondwana Research, v. 16, n. 2, p. 189–200, http://dx.doi.org/10.1016/j.gr.2009.03.002

Chen, H. L., Yang, S. F., Li, Z. L., Yu, X., Xiao, W. J., Yuan, C., Lin, X. B., and Li, J. L., 2006, Zircon SHRIMP U-Pb chronology of Fuyun basic granulite and its tectonic significance in Altaid orogenic belt: Acta Petrologica Sinica, v. 22, n. 5, p. 1351–1358 (in Chinese with English Abstract).

Chen, L. H., and Han, B. F., 2006, Geochronology, geochemistry and Sr-Nd-Pb isotopic composition of mafic intrusive rocks in Wuqiagou area, north Xinjiang: Constraints for mantle sources and deep processes: Acta Petrologica Sinica, v. 22, n. 5, p. 1201–1214 (in Chinese with English Abstract).

Choulet, F., Faure, M., Cluzel, D., Chen, Y., Lin, W., and Wang, B., 2012, From oblique accretion to transpression in the evolution of the Altaid collage: New insights from West Junggar, northwestern China: Gondwana Research, v. 21, n. 2–3, p. 530–547, http://dx.doi.org/10.1016/j.gr.2011.07.015

Chu, N. C., Taylor, R. N., Chavagnac, V., Nesbitt, R. W., Boella, R. M., Milton, J. A., German, C. R., Bayon, G., and Burton, K., 2002, Hf isotope ratio analysis using multi-collector inductively coupled plasma mass spectrometry: an evaluation of isobaric interference corrections: Journal of Analytical Atomic Spectrometry, v. 17, p. 1567–1574, http://dx.doi.org/10.1039/b206707b

Elhlou, S., Belousova, E., Griffin, W. L., Pearson, N. J., and O'Reilly, S. Y., 2006, Trace element and isotopic composition of GJ-red zircon standard by laser ablation: Geochimica et Cosmochimica Acta, v. 70, n. 18, p. A158–A158, http://dx.doi.org/10.1016/j.gca.2006.06.1383

Gao, F. P., Zhou, G., Lei, Y. X., Wang, D. S., Chen, J. X., Zhang, H. F., Wu, X. B., Liu, G. R., and Zhao, Z. H., 2010, Early Permian granite age and geochemical characteristics in Shaerbulake of Xinjiang's Altay area and its geological significance: Geological Bulletin of China, v. 29, n. 9, p. 1281–1293 (in Chinese with English Abstract).

Gao, J. F., and Zhou, M. F., 2013a, Magma mixing in the genesis of the Kalatongke dioritic intrusion: Implications for the tectonic switch from subduction to post-collision, Chinese Altay, NW China: Lithos, v. 162–163, p. 236–250, http://dx.doi.org/10.1016/j.lithos.2013.01.007

——— 2013b, Generation and evolution of siliceous high magnesium basaltic magmas in the formation of the Permian Huangshandong intrusion (Xinjiang, NW China): Lithos, v. 162–163, p. 128–139, http://dx.doi.org/10.1016/j.lithos.2013.01.002

Gao, J. F., Zhou, M. F., Lightfoot, P. C., and Qu, W., 2012a, Heterogeneous Os isotope compositions in the Kalatongke sulfide deposit, NW China: the role of crustal contamination: Mineralium Deposita, v. 47, n. 7, p. 731–738, http://dx.doi.org/10.1007/s00126-012-0414-7

Gao, J. F., Zhou, M. F., Lightfoot, P. C., Wang, C. Y., and Qi, L., 2012b, Origin of PGE-poor and Cu-rich magmatic sulfides from the Kalatongke deposit, Xinjiang, Northwest China: Economic Geology, v. 107, n. 3, p. 481–506, http://dx.doi.org/10.2113/econgeo.107.3.481

Geng, H. Y., Sun, M., Yuan, C., Xiao, W. J., Xian, W. S., Zhao, G. C., Zhang, L. F., Wong, K., and Wu, F. Y., 2009, Geochemical, Sr-Nd and zircon U-Pb-Hf isotopic studies of Late Carboniferous magmatism in the West Junggar, Xinjiang: Implications for ridge subduction?: Chemical Geology, v. 266, n. 3–4, p. 364–389, http://dx.doi.org/10.1016/j.chemgeo.2009.07.001

Gong, H. L., Chen, Z. L., Hu, Y. Q., Li, L., Lai, X. R., Ma, Q. Y., Li, Y. Y., Hu, B., and Zhang, W. G., 2007, Geochemical characteristics of acidic dike swarm from the eastern segment of the Ertix tectonic belt, Altai orogeny and its geological implications: Acta Petrologica Sinica, v. 23, n. 5, p. 889–899 (in Chinese with English Abstract).

Griffin, W. L., Wang, X., Jackson, S. E., Pearson, N. J., O'Reilly, S. Y., Xu, X. S., and Zhou, X. M., 2002, Zircon chemistry and magma mixing, SE China: *In-situ* analysis of Hf isotopes, Tonglu and Pingtan igneous complexes: Lithos, v. 61, n. 3–4, p. 237–269, http://dx.doi.org/10.1016/S0024-4937(02)00082-8

Han, B. F., Wang, S. G., Jahn, B. M., Hong, D. W., Kagami, H., and Sun, Y. L., 1997, Depleted-mantle source for the Ulungur River A-type granites from North Xinjiang, China: geochemistry and Nd-Sr isotopic

evidence, and implications for Phanerozoic crustal growth: Chemical Geology, v. 138, n. 3–4, p. 135–159, http://dx.doi.org/10.1016/S0009-2541(97)00003-X

Han, B. F., Ji, J. Q., Song, B., Chen, L. H., and Li, Z. H., 2004, SHRIMP zircon U-Pb ages of Kalatongke No. 1 and Huangshandong Cu-Ni-bearing mafic-ultramafic complexes, North Xinjiang, and geological implications: Chinese Science Bulletin, v. 49, n. 22, p. 2424–2429 (in Chinese).

Han, B. F., Ji, J. Q., Song, B., Chen, L. H., and Zhang, L., 2006, Late Paleozoic vertical growth of continental crust around the Junggar Basin, Xinjiang, China (Part I): Timing of post-collisional plutonism: Acta Petrologica Sinica, v. 22, n. 5, p. 1077–1086 (in Chinese with English Abstract).

Han, B. F., Guo, Z. J., Zhang, Z. C., Zhang, L., Chen, J. F., and Song, B., 2010, Age, geochemistry, and tectonic implications of a late Paleozoic stitching pluton in the North Tian Shan suture zone, western China: Geological Society of American Bulletin, v. 122, n. 3–4, p. 627–640, http://dx.doi.org/10.1130/B26491.1

Han, B. F., He, G. Q., Wang, X. C., and Guo, Z. J., 2011, Late Carboniferous collision between the Tarim and Kazakhstan–Yili terranes in the western segment of the South Tian Shan Orogen, Central Asia, and implications for the Northern Xinjiang, western China: Earth-Science Reviews, v. 109, n. 3–4, 74–93, http://dx.doi.org/10.1016/j.earscirev.2011.09.001

He, G. Q., Han, B. F., Yue, Y. J., and Wang, J. H., 1990, Tectonic division and crustal evolution of Altay Orogenic Belt in China: Geoscience (Xinjiang), v. 2, p. 9–20 (in Chinese with English Abstract).

Hong, D. W., Wang, S. G., Han, B. F., and Jin, M. Y., 1994, The Permian alkaline granites in Central Inner Mongolia and their geodynamic significance: Journal of Southeast Asian Earth Sciences, v. 10, n. 3–4, 169–176, http://dx.doi.org/10.1016/0743-9547(94)90017-5

Hou, K. J., Li, Y. H., Zou, T. R., Qu, X. M., Shi, Y. R., and Xie, G. Q., 2007, Laser ablation-MC-ICP-MS technique for Hf isotope microanalysis of zircon and its geological applications: Acta Petrologica Sinica, v. 23, n. 10, p. 2595–2604 (in Chinese with English Abstract).

Hu, A. Q., Wei, G. J., Deng, W. F., and Chen, L. L., 2006, SHRIMP zircon U-Pb dating and its significance for gneisses from the southwest area to Qinghe County in the Altai, China: Acta Petrologica Sinica, v. 22, n. 1, p. 1–10 (in Chinese with English Abstract).

Jahn, B. M., 2004, The Central Asian Orogenic Belt and growth of the continental crust in the Phanerozoic, *in* Malpas, J., Fletcher, C. J. N., Ali, J. R., and Aitchison, J. C., editors, Aspects of the Tectonic Evolution of China: Geological Society, Special Publications, London, v. 226, p. 73–100, http://dx.doi.org/10.1144/GSL.SP.2004.226.01.05

Jahn, B. M., Wu, F. Y., and Chen, B., 2000a, Granitoids of the Central Asian Orogenic belt and continental growth in the Phanerozoic: Transactions of the Royal Society of Edinburgh: Earth Sciences, v. 91, n. 1–2, p. 181–193, http://dx.doi.org/10.1017/S0263593300007367

——— 2000b, Massive granitoid generation in Central Asia: Nd isotope evidence and implication for continental growth in the Phanerozoic: Episodes, v. 23, p. 82–92.

Jahn, B. M., Litvinovskyb, B. A., Zanvilevichb, A. N., and Reichowc, M., 2009, Peralkaline granitoid magmatism in the Mongolian–Transbaikalian Belt: Evolution, petrogenesis and tectonic significance: Lithos, v. 113, n. 3–4, p. 521–539, http://dx.doi.org/10.1016/j.lithos.2009.06.015

Jian, P., Liu, D. Y., Zhang, Q., Zhang, F. Q., Shi, Y. R., Shi, G. H., Zhang, L. Q., and Tao, H., 2003, SHRIMP dating of ophiolite and leucocratic rocks within ophiolite: Earth Science Frontiers, v. 10, n. 10, p. 440–456 (in Chinese with English Abstract).

Jian, P., Liu, D. Y., Kröner, A., Windley, B. F., Shi, Y. R., Zhang, W., Miao, L. C., Zhang, L. Q., and Tomurhuu, D., 2010, Evolution of a Permian intraoceanic arc-trench system in the Solonker suture, Central Asian Orogenic Belt, China and Mongolia: Lithos, v. 118, n. 1–2, p. 169–190, http://dx.doi.org/10.1016/j.lithos.2010.04.014

Jiang, Y. D., Sun, M., Zhao, G. C., Yuan, C., Xiao, W. J., Xia, X. P., Long, X. P., and Wu, F. Y., 2010, The ~390 Ma high-*T* metamorphic event in the Chinese Altai: A consequence of ridge-subduction?: American Journal of Science, v. 310, n. 10, p. 1421–1452, http://dx.doi.org/10.2475/10.2010.08

Keto, L. S., and Jacobsen, S. B., 1987, Nd and Sr isotopic variations of Early Paleozoic oceans: Earth and Planetary Science Letters, v. 84, n. 1, p. 27–41, http://dx.doi.org/10.1016/0012-821X(87)90173-7

Khain, E. V., Bibikova, E. V., Salnikova, E. B., Kröner, A., Gibsher, A. S., Didenko, A. N., Degtyarev, K. E., and Fedotova, A. A., 2003, The Palaeo-Asian ocean in the Neoproterozoic and early Paleozoic: new geochronologic data and palaeotectonic reconstructions: Precambrian Research, v. 122, n. 1–4, p. 329–358, http://dx.doi.org/10.1016/S0301-9268(02)00218-8

Konopelko, D., Biske, G., Seltmann, R., Eklund, O., Belyatsky, B., 2007, Hercynian post-collisional A-type granites of the Kokshaal Range, Southern Tien Shan, Kyrgyzstan: Lithos, v. 97, n. 1–2, p. 140–160, http://dx.doi.org/10.1016/j.lithos.2006.12.005

Kovalenko, V. I., Yarmolyuk, V. V., Kovach, V. P., Kotov, A. B., Kozakov, I. K., Salnikova, E. B., and Larin, A. M., 2004, Isotope provinces, mechanisms of generation and sources of the continental crust in the Central Asian Mobile Belt: geological and isotopic evidence: Journal of Asian Earth Sciences, v. 23, n. 5, p. 605–627, http://dx.doi.org/10.1016/S1367-9120(03)00130-5

Kröner, A., Windley, B. F., Badarch, G., Tomurtogoo, O., Hegner, E., Jahn, B. M., Gruschka, S., Khain, E. V., Demoux, A., and Wingate, M. T. D., 2007, Accretionary growth and crust formation in the Central Asian orogenic belt and comparison with the Arabian-Nubian shield, *in* Hatcher, R. D., Carlson M. P., McBride J. H., and Martínez Catalán, J. R., editors, 4-D Framework of Continental Crust: Geological Society of America Memoirs, v. 200, p. 181–209, http://dx.doi.org/10.1130/2007.1200(11)

Kröner, A., Kovach, V., Belousova, E., Hegner, E., Armstrong, R., Dolgopolova, A., Seltmann, R., Alexeiev, D. V., Hoffmann, J. E., Wong, J., Sun, M., Cai, K., Wang, T., Tong, Y., Wilde, S. A., Degtyarev, K. E., and Rytsk, E., 2013, Reassessment of continental growth during the accretionary history of the Central Asian Orogenic Belt: Gondwana Research, v. 25, n. 1, p. 103–125, http://dx.doi.org/10.1016/j.gr.2012.12.023

Laurent-Charvet, S., Charvet, J., Monié, P., and Shu, L., 2003, Late Paleozoic strike-slip shear zones in eastern

central Asia (NW China): New structural and geochronological data: Tectonics, v. 22, n. 2, p. 1009, http://dx.doi.org/10.1029/2001TC901047

Le Maitre, R. W., Bateman, P., Dudek, A., Keller, J., Le Bas, M. J., Sabine, P. A., Schmid, R., Sorensen, H., Streckeisen, A., Woolley, A. R., and Zanettin, B., 1989, Igneous rocks: A classification of and glossary of terms: Oxford, Blackwell, 193 p.

Li, J. Y., 1995, Main characteristics and emplacement processes of the east Junggar ophiolites, Xinjiang, China: Acta Petrologica Sinica, v. 5, p. 73–84 (in Chinese with English Abstract).

Li, J. Y., Xiao, W. J., Wang, K. Z., Sun, G. H., and Gao, L. M., 2003, Neoproterozoic-Palaeozoic tectonostratigraphy, magmatic activities and tectonic evolution of eastern Xinjiang, NW China, *in* Mao J. W., Goldfarb, R. J., Seltman, R., Wang, D. H., Xiao, W. J., and Hart, C., editors, Tectonic Evolution and Metallogeny of the Chinese Altay and Tianshan: London, IAGOD Guidebook, Series 10, CERCAM/NHM, p. 31–74.

Li, X. R., Liu, F., and Yang, F. Q., 2012, Geological times and its signification of the two mica syenogranite in the Keyinblak Cu-Zn deposit area in Altay, Xinjiang: Xinjiang Geology, v. 30, n. 1, p. 5–11 (in Chinese with English Abstract).

Li, Z. H., Han, B. F., and Song, B., 2004, SHRIMP zircon U-Pb dating of the Ertaibei granodiorite and its enclave from eastern Junggar, Xinjiang, and geological implications: Acta Petrologica Sinica, v. 20, n. 5, p. 1263–1270 (in Chinese with English Abstract).

Li, Z. L., Li, Y. Q., Chen, H. L., Santosh, M., Yang, S. F., Xu, Y. G., Langmuir, C. H., Chen, Z. X., Yu, X., and Zou, S. Y., 2011, Hf isotopic characteristics of the Tarim Permian large igneous province rocks of NW China: Implication for the magmatic source and evolution: Journal of Asian Earth Sciences, v. 49, p. 191–202, http://dx.doi.org/10.1016/j.jseaes.2011.11.021

Liu, J. Y., Yuan, K. R., Wu, G. Q., Xin, J. G., and Liu, S., 1996, A study on alkali-rich granitoids and related mineralization in eastern Junggar, Xinjiang, China: Changsha, Central South University Press, p. 13–170 (in Chinese).

Liu, W., Liu, X. J., and Xiao, W. J., 2012, Massive granitoid production without massive continental-crust growth in the Chinese Altay: Insight into the source rock of granitoids using integrated zircon U-Pb age, Hf-Nd-Sr isotopes and geochemistry: American Journal of Science, v. 312, n. 6, p. 629–684, http://dx.doi.org/10.2475/06.2012.02

Long, X. P., Sun, M., Yuan, C., Xiao, W. J., Lin, S. F., Wu, F. Y., Xia, X. P., and Cai, K. D., 2007, Detrital zircon age and Hf isotopic studies for metasedimentary rocks from the Chinese Altai: Implications for the Early Paleozoic tectonic evolution of the Central Asian Orogenic Belt: Tectonics, v. 26, n. 5, TC5015, http://dx.doi.org/doi: 10.1029/2007TC002128

Long, X. P., Sun, M., Yuan, C., Xiao, W. J., and Cai, K. D., 2008, Early Paleozoic sedimentary record of the Chinese Altai: Implications for its tectonic evolution: Sedimentary Geology, v. 208, n. 3–4, p. 88–100, http://dx.doi.org/10.1016/j.sedgeo.2008.05.002

Long, X. P., Yuan, C., Sun, M., Xiao, W. J., Zhao, G. C., Wang, Y. J., Cai, K. D., Xia, X. P., and Xie, L. W., 2010, Detrital zircon ages and Hf isotopes of the early Paleozoic flysch sequence in the Chinese Altai, NW China: New constrains on depositional age, provenance and tectonic evolution: Tectonophysics, v. 480, n. 1–4, p. 213–231, http://dx.doi.org/10.1016/j.tecto.2009.10.013

Lu, S. N., Li, H. K., Li, H. M., Song, B., Wang, S. Y., Zhou, H. Y., Chen, Z. H., 2003, U-Pb isotopic ages and their significance of Alkaline Granite in the southern margin of the North China Craton: Geological Bulletin of China, v. 22, n. 12, p. 762–768 (in Chinese with English abstract).

Ludwig, K. R., 2003, A geochronological toolkit for Microsoft Excel: Berkeley, California, Berkeley Geochronology Center, Special Publication, v. 4, p. 25–32.

Maniar, P. D., and Piccoli, P. M., 1989, Tectonic discrimination of granitoids: Geological Society of America Bulletin, v. 101, n. 5, p. 635–643, http://dx.doi.org/10.1130/0016-7606(1989)101⟨0635:TDOG⟩2.3.CO;2

Mao, J. W., Pirajno, F., Zhang, Z. H., Chai, F. M., Yang, J. M., Wu, H., Chen, S. P., Cheng, S. L., and Zhang, C. Q., 2006, Late Variscan post-collisional Cu-Ni sulfide deposits in East Tianshan and Altay in China: Principal characteristics and possible relationship with mantle plume: Acta Geologica Sinica, v. 80, n. 7, p. 925–946 (in Chinese with English abstract).

Niu, H. C., Sato, H., Zhang, H. X., Ito, J., Nagao, T., Yu, X. Y., Terada, K., and Zhang, Q., 2006, Juxtaposition of adakite, boninite, high-TiO_2 and low-TiO_2 basalts in the Devonian southern Altay Xinjiang NW China: Journal of Asian Earth Science, v. 28, n. 4–6, p. 439–456, http://dx.doi.org/10.1016/j.jseaes.2005.11.010

Pearce, J. A., Harris, N. B. W., and Tindle, A. G., 1984, Trace element discrimination diagrams for the tectonic interpretation of granitic rocks: Journal of Petrology, v. 25, n. 4, p. 956–983, http://dx.doi.org/10.1093/petrology/25.4.956

Pirajno F., 2010, Intracontinental strike-slip faults, associated magmatism, mineral systems and mantle dynamics: examples from NW China and Altay-Sayan (Siberia): Journal of Geodynamics, v. 50, n. 3–4, p. 325–346, http://dx.doi.org/10.1016/j.jog.2010.01.018

Pirajno, F., Seltmann, R., and Yang, Y. Q., 2011, A review of mineral systems and associated tectonic settings of northern Xinjiang, NW China: Geoscience Frontiers, v. 2, n. 2, p. 157–185, http://dx.doi.org/10.1016/j.gsf.2011.03.006

Qiao, G. S., 1988, Normalization of isotopic dilution analyses — a new program for isotope mass spectrometric analysis: Scientia Sinica (Series A), v. 31, n. 10, p. 1263–1268 (in Chinese).

Ren, B. Q., Zhang, H., Tang, Y., and Lu Z. H., 2011, LA-ICPMS U-Pb zircon geochronology of the Altai pegmatites and its geological significance: Acta Mineralogica Sinica, v. 31, n. 3, p. 587–596 (in Chinese with English Abstract).

Sengör, A. M. C., and Natal'in, B. A., 1996, Paleotectonics of Asia: fragments of a synthesis, *in* Yin, A., and Harrison, M., editors, The Tectonic Evolution of Asia: Cambridge, Cambridge University Press, p. 486–640.

Şengör, A. M. C., Natal'in, B. A., and Burtman, V. S., 1993, Evolution of Altaid tectonic collage and Paleozoic crustal growth in Eurasia: Nature, v. 364, p. 299–307, http://dx.doi.org/10.1038/364299a0

Shan, Q., Niu, H. C., Yu, X. Y., and Zhang, H. X., 2005, Geochemistry and zircon U-Pb age of volcanic rocks from the Hanasi basin in the northern Xinjiang and their tectonic significance: Geochimica, v. 34, n. 4, p. 315–327 (in Chinese with English Abstract).

Söderlund, U., Patchett, J. P., Vervoort, J. D., and Isachsen, C. E., 2004, The ^{176}Lu decay constant determined by Lu-Hf and U-Pb isotope systematics of Precambrian mafic intrusions: Earth and Planetary Science Letters, v. 219, n. 3–4, p. 311–324, http://dx.doi.org/10.1016/S0012-821X(04)00012-3

Song, X. Y., and Li, X. R., 2009, Geochemistry of the Kalatongke Ni-Cu-(PGE) sulfide deposit, NW China: implications for the formation of magmatic sulfide mineralization in a postcollisional environment: Mineralium Deposita, v. 44, n. 3, p. 303–327, http://dx.doi.org/10.1007/s00126-008-0219-x

Stacey, J. S., and Kramers, J. D., 1975, Approximation of terrestrial lead isotope evolution by a two-stage model: Earth and Planetary Science Letters, v. 26, n. 2, p. 207–221, http://dx.doi.org/10.1016/0012-821X(75)90088-6

Sun, G. H., Li, J. Y., Yang, T. N., Li, Y. P., Zhu, Z. X., and Yang, Z. Q., 2009a, Zircon SHRIMP U-Pb dating of two linear granite plutons in southern Altay Mountains and its tectonic implications: Geology in China, v. 36, n. 5, p. 976–987 (in Chinese with English Abstract).

Sun, M., Long, X. P., Cai, K. D., Jiang, Y. D., Wang, B. Y., Yuan, C., Zhao, G. C., Xiao, W. J., and Wu, F. Y., 2009b, Early Paleozoic ridge subduction in the Chinese Altai: Insight from the abrupt change in zircon Hf isotopic compositions: Science in China Series, D: Earth Sciences, v. 52, n. 9, p. 1345–1348, doi: 10.1007/s11430-009-0110-3

Sun, M., Yuan, C., Xiao, W. J., Long, X. P., Xia, X., Zhao, G. C., Lin, S. F., Wu, F. Y., and Kröner, A., 2008, Zircon U-Pb and Hf isotopic study of gneissic rocks from the Chinese Altai: Progressive accretionary history in the early to middle Palaeozoic: Chemical Geology, v. 247, n. 3–4, p. 352–383, http://dx.doi.org/10.1016/j.chemgeo.2007.10.026

Sun, S., and McDonough, W. F., 1989, Chemical and isotopic systematics of oceanic basalts: implications for mantle compositions and processes: Geological Society, London, Special Publications, v. 42, p. 313–45, http://dx.doi.org/10.1144/GSL.SP.1989.042.01.19

Tong, Y., Wang, T., and Hong, D. W., 2005, Zircon U-Pb age of Tielike pluton in the western Altai orogen and its implications: Acta Geoscientia Sinica, v. 26, p. 74–77 (in Chinese with English Abstract).

Tong, Y., Wang, T., Hong, D. W., Dai, Y. J., Han, B. F., and Liu, X. M., 2007, Ages and origin of the early Devonian granites from the north part of Chinese Altai Mountains and its tectonic implications: Acta Petrologica Sinica, v. 23, n. 8, p. 1933–1944 (in Chinese with English abstract).

Tong, Y., Wang, T., Hong, D. W., Wang, S. G., and Han, B. F., 2006a, TIMS U-Pb zircon ages of Fuyun post-orogenic linear granite plutons on the southern margin of Altay orogenic belt and their implications: Acta Petrologica et Mineralogica, v. 25, n. 2, p. 85–89 (in Chinese with English abstract).

Tong, Y., Wang, T., Kovach, V. P., Hong, D. W., and Han, B. F., 2006b, Age and origin of the Takeshiken Postorogenic alkali-rich intrusive rocks in southern Altai, near the Mongolian border in China and its implications for continental growth: Acta Petrologica Sinica, v. 22, n. 5, p. 1267–1278 (in Chinese with English abstract).

Tong, Y., Wang, T., Hong, D. W., Han, B. F., Zhang, J. J., Shi, X. J., and Wang, C., 2010, Spatial and temporal distribution of the Carboniferous-Permian granitoids in the Northern Xinjiang and its adjacent areas, and its tectonic significance: Acta Petrologica et Mineralogica, v. 2, n. 6, p. 619–641 (in Chinese with English abstract).

Tong, Y., Wang, T., Siebel, W., Hong, D. W., and Sun, M., 2012, Recognition of early Carboniferous alkaline granite in the southern Altai orogen: post-orogenic processes constrained by U-Pb zircon ages, Nd isotopes, and geochemical data: International Journal of Earth Sciences, v. 101, n. 4, p. 937–950, http://dx.doi.org/10.1007/s00531-011-0700-0

Travin, A. V., Boven, A., Plotnikov, A. V., Vladimirov, V. G., Theunissen, K., Vladimirov, A. G., Melnikov, A. I., and Titov, A. V., 2001, Ar-40/Ar-39 dating of ductile deformations in the Irtysh shear zone, eastern Kazakhstan: Geochemistry International, v. 39, n. 12, p. 1237–1241.

Turner, S. P., Foden, J. D., and Morrison, R. S., 1992, Derivation of some A-type magmas by fractionation of basaltic magma: an example from the Padthaway Ridge, South Australia: Lithos, v. 28, n. 2, p. 151–179, http://dx.doi.org/10.1016/0024-4937(92)90029-X

Wang, T., Hong, D. W., Tong, Y., Han, B. F., and Shi, Y. R., 2005, Zircon U-Pb SHRIMP age and origin of post-orogenic Lamazhou granitic pluton from Chinese Altai Orogen: its implications for vertical continental growth: Acta Petrologica Sinica, v. 21, p. 640–650 (in Chinese with English abstract).

Wang, T., Hong, D. W., Jahn, B. M., Tong, Y., Wang, Y. B., Han, B. F., and Wang, X. X., 2006, Timing, petrogenesis, and setting of Palaeozoic synorogenic intrusions from the Altai Mountains, northwest China: Implications for the tectonic evolution of an accretionary orogen: The Journal of Geology, v. 114, n. 6, p. 735–751, http://dx.doi.org/10.1086/507617

Wang, T., Tong, Y., Jahn, B. M., Zou, T. R., Wang, Y. B., Hong, D. W., and Han, B. F., 2007, SHRIMP U-Pb zircon geochronology of the Altai No. 3 Pegmatite, NW China, and its implications for the origin and tectonic setting of the pegmatite: Ore Geology Reviews, v. 32, n. 1–2, p. 325–336, http://dx.doi.org/10.1016/j.oregeorev.2006.10.001

Wang, T., Jahn, B. M., Kovach, V. P., Tong, Y., Hong, D. W., and Han, B. F., 2009a, Nd-Sr isotopic mapping of the Chinese Altai and implications for continental growth in the Central Asian Orogenic Belt: Lithos, v. 110, n. 1–4, p. 359–372, http://dx.doi.org/10.1016/j.lithos.2009.02.001

Wang, T., Tong, Y., Li, S., Zhang, J. J, Shi, X. J., Li, J. Y., Han, B. F., and Hong, D. W., 2010, Spatial and temporal variations of granitoids in the Altai orogen and their implications for tectonic setting and crustal growth: examples from the Chinese Altai: Acta Petrologica et Mineralogica, v. 29, n. 6, p. 595–618 (in Chinese with English Abstract).

Wang, T., Jahn, B. M., Kovach, V. P., Tong, Y., Wilde, S. A., Hong, D. W., Li, S., and Salnikova, E. B., 2013, Mesozoic intraplate granitic magmatism in the Altai accretionary orogen, NW China: Implications for crustal architecture and growth: American Journal of Science, v. 314, n. 1, p. 1–42, http://dx.doi.org/10.2475/01.2014.01

Wang, W., Wei, C. J., Wang, T., Lou, Y. X., and Chu, H., 2009b, Confirmation of pelitic granulite in the Altai orogen and its geological significance: Chinese Science Bulletin, v. 54, n. 14, p. 2543–2548, http://dx.doi.org/10.1007/s11434-009-0041-6

Wang, Y. J., Yuan, C., Long, X. P., Sun, M., Xiao, W. J., Zhao, G. C., Cai, K. D., and Jiang, Y. D., 2011, Geochemistry, zircon U-Pb ages and Hf isotopes of the Paleozoic volcanic rocks in the northwestern Chinese Altai: Petrogenesis and tectonic implications: Journal of Asian Earth Sciences, v. 42, n. 5, p. 969–985, http://dx.doi.org/10.1016/j.jseaes.2010.11.005

Wei, C. J., Clarke, G., Tian, W., and Qiu, L., 2007, Transition of metamorphic series from the Kyanite- to andalusite-types in the Altai orogen, Xinjiang, China: Evidence from petrography and calculated KMnFMASH and KFMASH phase relations: Lithos, v. 96, n. 3–4, p. 353–374, http://dx.doi.org/10.1016/j.lithos.2006.11.004

Wilhem, C., Windley, B. F., and Stampfli, G. M., 2012, The Altaids of Central Asia: A tectonic and evolutionary innovative review: Earth Science Reviews, v. 113, n. 3–4, p. 303–341, http://dx.doi.org/10.1016/j.earscirev.2012.04.001

Williams, I. S., 1998, U-Th-Pb Geochronology by Ion Microprobe, *in* McKibben, M. A., Shanks III, W. C., and Ridley, W. I., editors, Applications of microanalytical techniques to understanding mineralizing processes: Reviews in Economic Geology, v. 7. p. 1–35.

Windley, B. F., Kroner, A., Guo, J. H., Qu, G. S., Li, Y., and Zhang, C., 2002, Neoproterozoic to Palaeozoic geology of the Altai orogen, NW China: New zircon age data and tectonic evolution: The Journal of Geology, v. 110, n. 6, p. 719–737, http://dx.doi.org/10.1086/342866

Windley, B. F., Alexeiev, D., Xiao, W. J., Kroner, A., and Badarch, G., 2007, Tectonic models for accretion of the Central Asian Orogenic Belt, Bicentennial Review: Journal of the Geological Society, London, v. 164, n. 1, p. 31–47, doi: 10.1144/0016-76492006-022

Wong, K., Sun, M., Zhao, G. C., Yuan, C., and Xiao, W. J., 2010, Geochemical and geochronological studies of the Alegedayi Ophiolitic Complex and its implication for the evolution of the Chinese Altai: Gondwana Research, v. 18, n. 2–3, p. 438–454, http://dx.doi.org/10.1016/j.gr.2010.01.010

Wu, F. Y., Yang, Y. H., Xie, L. W., Yang, J. H., and Xu, P., 2006, Hf isotopic compositions of the standard zircons and baddeleyites used in U-Pb geochronology: Chemical Geology, v. 234, n. 1–2, p. 105–126, http://dx.doi.org/10.1016/j.chemgeo.2006.05.003

Xiao, W. J., Windley, B. F., Hao, J., and Zhai, M. G., 2003, Accretion leading to collision and the Permian Solonker suture, Inner Mongolia, China: Termination of the central Asian orogenic belt: Tectonics, v. 22, n. 6, p. 1014, http://dx.doi.org/10.1029/2002TC001484

Xiao, W. J., Windley, B. F., Badararch, G., Sun, S., Li, J., Qin, K., and Wang, Z., 2004, Paleozoic accretionary and convergent tectonics of the southern Altaids: implications for the growth of central Asia: Journal of the Geological Society, London, v. 161, n. 3, p. 339–342, http://dx.doi.org/10.1144/0016-764903-165

Xiao, W. J., Han, C. M., Yuan, C., Sun, M., Lin, S. F., Chen, H. L., Li, Z. L., Li, J. L., and Sun, S., 2008, Middle Cambrian to Permian subduction-related accretionary orogenesis of Northern Xinjiang, NW China: Implications for the tectonic evolution of central Asia: Journal of Asian Earth Sciences, v. 32, n. 2–4, p. 102–117, http://dx.doi.org/10.1016/j.jseaes.2007.10.008

Xiao, W. J., Kröner, A., and Windley, B. F., 2009a, Geodynamic evolution of Central Asia in the Paleozoic and Mesozoic: International Journal of Earth Sciences, v. 98, n. 6, p. 1185–1188, http://dx.doi.org/10.1007/s00531-009-0418-4

Xiao, W. J., Windley, B. F., Yuan, C., Sun, M., Han, C. M., Lin, S. F., Chen, H. L., Yan, Q. R., Liu, D. Y., Qin, K. Z., Li J. L., and Sun, S., 2009b, Paleozoic multiple subduction-accretion processes of the southern Altaids: American Journal of Science, v. 309, n. 3, p. 221–270, http://dx.doi.org/10.2475/03.2009.02

Xiao, W. J., Huang, B. C., Han, C. M., Sun, S., and Li, J. L., 2010, A review of the western part of the Altaids: A key to understanding the architecture of accretionary orogens: Gondwana Research, v. 18, n. 2–3, p. 253–273, http://dx.doi.org/10.1016/j.gr.2010.01.007

Xu, J. F., Castillo, P. R., Chen, F. R., Niu, H. C., Yu, X. Y., and Zhen, Z. P., 2003, Geochemistry of late Paleozoic mafic igneous rocks from the Kuerti area, Xinjiang, northwest China: implications for backarc mantle evolution: Chemical Geology, v. 193, n. 1–2, p. 137–154, http://dx.doi.org/10.1016/S0009-2541(02)00265-6

Yakubchuk, A., 2004, Architecture and mineral deposit settings of the Altaid orogenic collage: a revised model: Journal of Asian Earth Sciences, v. 23, n. 5, p. 761–779, http://dx.doi.org/10.1016/j.jseaes.2004.01.006

Yang, G., Li, Y. J., Wu, H. G., Zhong, X., Yang, B. K., Yan, C. X., Yan, J., and Si, G. H., 2011b, Geochronological and geochemical constrains on petrogenesis of the Huangyangshan A-type granite from the East Junggar, Xinjiang, NW China: Journal of Asian Earth Sciences, v. 40, n. 3, p. 722–736, http://dx.doi.org/10.1016/j.jseaes.2010.11.008

Yang, T. N., Li, J. Y., Zhang, J., and Hou, K. J., 2011a, The Altai-Mongolia terrane in the Central Asian Orogenic Belt (CAOB): A peri-Gondwana one? Evidence from zircon U-Pb, Hf isotopes and REE abundance: Precambrian Research, v. 187, n. 1–2, p. 79–98, http://dx.doi.org/10.1016/j.precamres.2011.02.005

Yuan, C., Sun, M., Xiao, W. J., Li, X. H., Chen, H. L., Lin, S. F., Xia, X. P., and Long, X. P., 2007, Accretionary orogenesis of the Chinese Altai: Insights from Paleozoic granitoids: Chemical Geology, v. 242, n. 1–2, p. 22–39, http://dx.doi.org/10.1016/j.chemgeo.2007.02.013

Zhang, C. L., Xu, Y. G., Li, Z. X., Wang, H. Y., and Ye, H. M., 2010a, Diverse Permian magmatism in the Tarim

Block, NW China: Genetically linked to the Permian Tarim mantle plume?: Lithos, v. 119, n. 3–4, p. 537–552, http://dx.doi.org/10.1016/j.lithos.2010.08.007

Zhang, C. L., Li, Z. X., Li, X. H., Xu, Y. G., Zhou, G., and Ye, H. M., 2010b, A Permian large igneous province in Tarim and Central Asian orogenic belt, NW China: Results of a *ca.* 275 Ma mantle plume?: Geological Society of America Bulletin, v. 122, n. 11–12, p. 2020–2040, http://dx.doi.org/10.1130/B30007.1

Zhang, C. L., Santosh, M., Zou, H. B., Xu, Y. G., Zhou, G., Dong, Y. G., Ding, R. F., and Wang, H. Y., 2012, Revisiting the "Irtish tectonic belt": Implications for the Paleozoic tectonic evolution of the Altai orogen: Journal of Asian Earth Sciences, v. 50, p. 117–133, http://dx.doi.org/10.1016/j.jseaes.2012.02.016

Zhang, H. X., Niu, H. C., Terada, K., Yu, X. Y., Sato, H., and Ito, J., 2003, Zircon SHRIMP U-Pb dating on plagiogranite from Kuerti ophiolite in Altay, North Xinjiang: Chinese Science Bulletin, v. 48, n. 20, p. 2231–2235.

Zhang, J. H., Wang, J. B., and Ding, R. F., 2000, Characteristics and U-Pb ages of zircon in metavolcanics from the Kangbutiebao formation in the Altay orogen, Xinjiang: Regional Geology of China, v. 19, n. 3, p. 281–287 (in Chinese with English abstract).

Zhou, G., Zhang, Z. C., Luo, S. B., He, B., Wang, X., Yin, L. J., Zhao, H., Li, A. H., and He, Y. K., 2007a, Confirmation of high temperature strongly peraluminous Mayin'ebo granites in the south margin of Altay, Xinjiang: age, geochemistry and tectonic implications: Acta Petrologica Sinica, v. 23, n. 8, p. 9–20 (in Chinese with English abstract).

Zhou, G., Zhang, Z. C., Wang, X., Luo, S. B., He, B., and Zhang, X. L., 2007b, Zircon U-Pb SHRIMP and ^{40}Ar-^{39}Ar dating of the granitic mylonite in the Mayinebo fault belt of north Xinjiang and its geological significance: Acta Geologica Sinica, v. 81, n. 3, p. 359–369 (in Chinese with English abstract).

Zhou, G., Zhang, Z. C., Wu, G. G., Dong, L. H., He, Y. K., Dong, Y. G., He, L. X., Qin, J. H., Zhao, Z. H., and Liu, G. R., 2009, Postorogenic extension and continental growth of the northeastern margin of the Juggar: Evidences from petrography and geochemistry of the Hadansun intrusive complex: Acta Geologica Sinica, v. 83, n. 3, p. 331–346 (in Chinese with English abstract).